UNIVERSITEIT VAN PRETORIA
UNIVERSITY OF PRETORIA
YUNIBESITHI YA PRETORIA

IMPELLER FAULT DETECTION UNDER FLUCTUATING FLOW CONDITIONS USING ARTIFICIAL NEURAL NETWORKS

by

Amin Jami

Submitted in partial fulfilment of the requirement for the degree

Masters of Engineering (Mechanical)

in the

Faculty of Engineering, Built Environment and information Technology
Department of Mechanical and Aeronautical Engineering
UNIVERSITY OF PRETORIA
2016

IMPELLER FAULT DETECTION UNDER FLUCTUATING FLOW CONDITIONS USING ARTIFICIAL NEURAL NETWORKS

by

Amin Jami

Supervisor:	P. Stephan Heyns
Department:	Mechanical and Aeronautical Engineering
University:	University of Pretoria
Degree:	Masters of Engineering (Mechanical)

Keywords: Condition monitoring, Non-stationary operating conditions, Time-frequency analysis, Artificial neural networks, Fault diagnosis

Summary:

Maintenance of equipment at the required condition to ensure a reliable performance, as well as improvement of safety, are major concerns in the field of asset integrity management. Condition monitoring is a procedure that allows one to identify early signs of failures and implement efficient maintenance plans to eliminate the uncertainties in machine operation. In addition, vibration monitoring is known as a detection tool for early detection of degradation from the expected performance. It is often superior to other condition monitoring techniques, due to its high sensitivity and simplicity of implementation. Vibration analysis provides substantial information regarding the operating condition of components and aids to remedy problems. Therefore, it can be used to detect a wide range of fault conditions in rotating machinery, such as imbalance, misalignment of internal shafts, looseness, cracked shaft, gear failures, rolling element bearing damages, motor faults and impeller issues.

The primary intention of the research reported in this dissertation is to investigate the applicability of a neural network methodology for the detection and diagnosis of mechanical defects of impellers in centrifugal pumps. The study focuses on extracting

appropriate features from vibration signals associated with pump impellers and the performance of artificial neural networks (ANNs) using these features. The second intention is to enhance maintenance decisions regarding the actual impeller condition. This leads to a transition from time based preventive maintenance to condition based maintenance, and also improving the safety and reliability of pumping systems, as well as reducing unexpected and catastrophic failures. Hence, vibration analysis techniques are used as a principal tool to characterise the impeller conditions under flow variation, with the requirements of data collection, data processing, transformation and selection of essential features corresponding to the running condition.

This dissertation presents a study of current vibration analysis techniques to extract the required features, namely time based features, frequency based features and wavelet based features. An experimental setup is developed to measure the impeller vibration. The experiment is performed using seven impeller fault conditions such as crack and imbalance under fluctuating flow conditions to simulate non-stationary conditions in the system. Also, the evolution of features over varying flow rates are evaluated in order to identify features that contain fundamental information corresponding the fault characteristics. Moreover, the collected features form non-dimensional training data sets are used to train ANNs. Comparisons of different training algorithms, network hidden nodes and effectiveness of different transfer functions are performed to select the most appropriate parameters of networks.

Validation of the results prove that the accuracy of ANN prediction improves considerably by using decomposed vibration signals and energy based features. Comparison of the network accuracy based on wavelet packet transform (WPT) features with time analysis and frequency analysis based features, indicate that WPT-ANN lead to lower mean square errors and higher correlation coefficients, as well as shorter training times. The WPT-ANN model can save computational time and provides better diagnostic information, which can be effectively used for classification of impeller defects under non-stationary conditions.

Acknowledgements

I would like to express my sincere gratitude towards those that assisted and supported me along the way of my journey:

- Prof. P.S. Heyns, my study leader, for giving me the opportunity to study under his supervision in Centre of Asset Integrity Management (C-AIM), for his continuous support, motivation, patience, enthusiasm, and immense knowledge. I could not have imagined having better advisor and mentor for my Masters study.

- The Sasol Laboratory for Structural Mechanics at the University of Pretoria for providing the required facilities to complete my research.

- Special thanks to George Breitenbach and Herman Booysen for their assistance during the experimental tests.

- My friends, especially Paul van Niekerk, for their encouragement and understanding during the past two years.

- My parents and my sister Fahimeh for their support and encouragement during the tough stressful times. It would have not been possible for me to reach the finish line without family support.

I am grateful to the University of Pretoria (UP) and Centre of Asset Integrity Management, for the financial support that has allowed me to conduct and complete this study.

I also acknowledge the Eskom Power Plant Engineering Institute (EPPEI) in their support to create the test facilities used in this work.

Table of Contents

Nomenclature

f	Activation function
F_s	Sampling frequency
λ	Failure rate
S_s	Strouhal number
D	Dimension
$X(t)$	A time signal
$F(w)$	Fast Fourier transform
μ	Mean value
N_s	Sampling length
σ	Variance
ψ	Wavelet
E	Energy
K_t	Kurtosis
S_n	Skewness
C_r	Crest factor
S_t	Standard deviation
IF	Impulse factor

Abbreviations

AIM	Asset integrity management
ANN	Artificial neural networks
BPF	Blade passing frequency
CBM	Condition based maintenance
CM	Condition monitoring
FA	Frequency analysis
FP	Failure prediction
FT	Fourier transform
LM	Levenberg-Marquardt
MSE	Mean square error
MLP	Multi-layer perceptron
PM	Preventive maintenance
PD	Probability density
RBM	Reliability based maintenance
RCM	Reliability centred maintenance
RL	Reinforcement learning
RMS	Root mean square
rpm	Revolutions per minute
STFT	Short-time Fourier transform
SL	Supervised learning
TPM	Total productive maintenance
TCM	Tool condition monitoring
TFA	Time-frequency analysis
UL	Unsupervised learning
WVD	Wigner Ville distribution

1. Introduction

1.1. Background and Motivation

Asset integrity management (AIM) aspires to ensure the highest possible availability, maintainability and reliability in operating machines. AIM can be accomplished through the contribution of maintenance and operational plans based on reliability strategies. It encompasses effective maintenance to obtain high reliability, reduction of both maintenance cost and failure probability, as well as reducing the consequences of risk to people and the environment as much as possible. It also helps to minimise machine life cycle costs by utilizing effective maintenance strategies such as reliability centred maintenance (RCM), total productive maintenance (TPM) and condition based maintenance (CBM). These are also recognized as the approaches that minimize downtime and ensure the machine longevity (SGS, 2015).

TPM eliminates the factors which may cause performance drop. The aim is to achieve the highest productivity with the lowest maintenance costs. It separates the maintenance activities into three main levels. Level one needs to be done by operators and technicians, which lets them feel responsible for their role in production and maintenance activities. Level two needs to be carried out by maintenance staff and the third level by the manufacturer. In addition, RCM is an optimization method that specifies individual maintenance strategies for each piece of component in order to operate as it was designed for (Deepak Prabhakar & Jagathy Raj, 2014). On the other hand, CBM is a maintenance strategy that uses the actual condition of machines to decide if maintenance is necessary.

Rotating machinery such as pumps, fans, compressors, engines, motors, gearboxes and bearings are key equipment that are extensively used in industrial systems such as fluid power systems. As these systems are becoming more complex in design as well as operation, higher reliability, safety and production capabilities are required. Pumps, valves and actuators are the main components in fluid power systems with application in farming, forestry, food, agriculture, power plants and automotive industries. The required reliability depends on the role of these applications, where critical equipment which are vital to the plant process, require the highest reliability and availability. In addition, according to the U.S. electric power research energy institute 22 % of the electricity consumption of industrial motors may be attributed to pumps. Electric motors are responsible for 69 % of the total electricity consumption in industry, thus pumps are responsible for 15 % of the total electricity consumption in both European and American industries (Ahonen, 2011).

Common defects of the pump components like impeller and bearings derived from imbalance, misalignment and looseness issues, may cause undesired deviation from the expected performance. Therefore, detecting the presence of defects at the early stage of development can help to maintain pumps at the highest performance, and lead to a notable saving in energy consumption.

1.2. Fault Detection

Fault detection (FD) also known as "diagnosis and prognosis procedures", involves detection of faults as well as making decisions on how to deal with them. Abnormal conditions affect the demanded performance and desired reliability, which lead to lower efficiencies and an increase in the total operational cost. Also, failure of critical machine components in a system could cause catastrophic or unacceptable damage. Hence, FD can significantly reduce the maintenance costs and unscheduled shutdowns by provision of preventive maintenance, optimal replacement decisions and scheduled shutdowns.

FD methods are applied to several industrial applications to detect various types of faults. This allows maintenance teams to order parts in advance, schedule manpower or plan other repairs during the downtime, and perform an overall boost in effective performance during the life cycle. Condition monitoring (CM) is therefore considered as a powerful tool to extract the required data for the maintenance strategies and assists in fault detection and maintenance plans. In addition, vibration signals are widely used in condition monitoring of rotating machinery due to their high sensitivity in detecting defects.

Subsequently, interpretation of extracted data becomes an important issue. This stage can be implemented by experienced personnel, but usually this method may not be adequate enough to indicate satisfactory results due to its difficulty and dependency on experienced engineers. Thus, the automated fault diagnosis can be performed by intelligent fault diagnosis and prognosis systems. Intelligent systems utilize machine learning algorithms such as artificial neural networks attempt to combine CM data to predict the propagation of faults.

Based on the preceding discussion, this dissertation focuses on vibration based condition monitoring of impellers in centrifugal pumps. Performance of the relevant condition monitoring techniques are evaluated for their ability to train ANNs and distinguish failures at an early stage under fluctuating operating conditions.

1.3. Literature

1.3.1. Introduction

This section is organized as follows. Section 1.3.2 looks at vibration analysis aspects in condition monitoring of rotating machinery, to explore the role of vibration analysis in fault diagnosis in pumping systems. Section 1.3.3 reviews pumping systems and the relevant common potential failure modes. A short discussion about aspects of condition monitoring in pumping systems is provided. In addition, significant frequency characteristics of the vibration in rotary components, such as impellers and bearings, are studied. Section 1.3.4 provides a study about signal measurement and signal processing. Common methods of signal analysis are explored in three main domains, namely time, frequency and time-frequency respectively. Also, a list of prominent parameters in each analysis method is presented. Section 1.3.5 gives a background about intelligent systems and their superiority as failure prognostic tools. A brief study of machine learning and the common learning algorithms is prepared. In this section, neural networks as well as recent studies in this field are explored.

1.3.2. Condition Monitoring and Fault Diagnosis

Condition monitoring is a method in identification of the health status of assets while in operation. During this process any considerable changes to health status that could lead to a failure will be identified.

CM methods can be classified in two classes, condition checking (direct-methods) and trend monitoring (indirect-methods) (Jardine et al., 2005)(Neale & Woodley, 1978). Direct methods measure the performance of equipment at one time point while in operation. This method is adequate to check condition of several similar items of equipment that are in operation in order to compare the measured parameters. Measurement of volumetric loss is an example of performing direct methods. On the other hand, indirect methods such as vibration, measure the condition parameters during the operational time, and evaluate the data to identify any changes regard to health condition.

In addition, maintenance strategies can be effectively performed based on the information obtained from condition monitoring during machine life cycle. A normal bathtub curve presents machine failure rate λ (number of failures per unit of time) over the life cycle as shown in figure1.1.

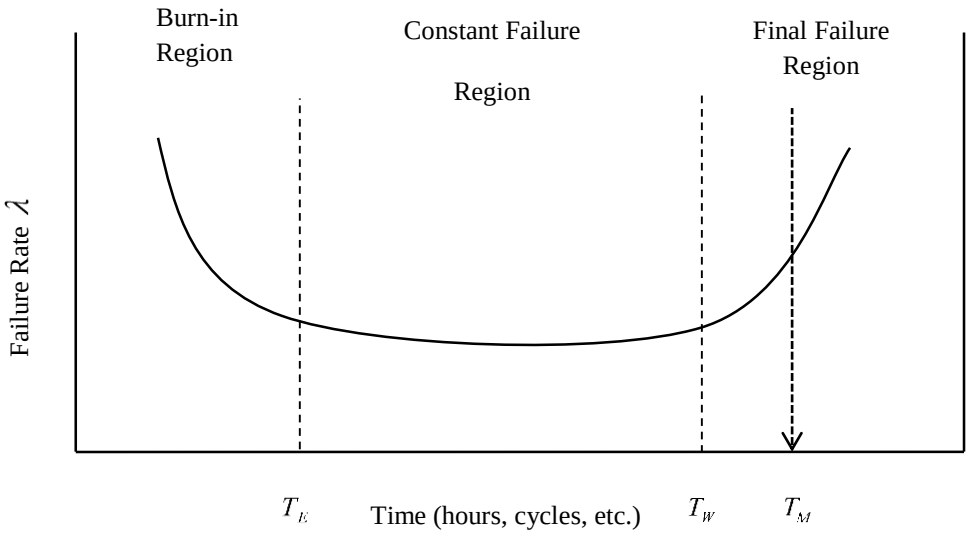

Figure 1.1. Bathtub curve and product failure behaviour (Bray & Stanley, 1997)

As shown in the figure 1.1, a failure rate curve consists of three main regions. The first "burn-in" region indicates early failures that are related to manufacturing defects. The constant failure and final failure regions are associated with time dependent operations of equipment in industry. As a typical failure rate is expected during the equipment life cycle, CM can determine if the equipment is running as expected by revealing the reliability level $R(t)$ which is a time (t) dependent function.

$$R(t) = e^{-\lambda t} \tag{1.1}$$

Girdhar introduces vibration monitoring as the most effective technique to identify the presence of potential failures in rotating machinery among other monitoring tools (Girdhar, 2004). A potential failure is a detectable condition that shows the occurrence of failure. Therefore, the stages of failure can be illustrated as a P-F curve (figure 1.2) which is an essential and cost saving tool for a RCM plan.

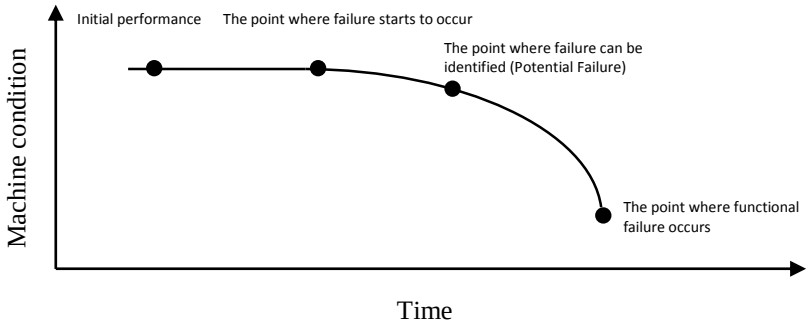

Figure 1.2. The P-V curve (Potential to functional failure (Moubray, 1992))

The intention of a P-F curve is to present how a machine fails and how early detection provides time before final functional failure occurs. Failures begin to occur as the machine operates, but unfortunately these signs are initially not detectable. Thereby, failure signs become detectable by growing defect sizes at a certain time using monitoring methods. Figure 1.2 illustrates how machine performance drops over a period of time, where the vertical axis denotes machine condition and the horizontal axis represents time.

The main concern on using the P-V curve is to identify the interval between a potential failure point and functional failure to be able to schedule maintenance before the total system fails completely. Figure 1.3 shows how failure signs can be detected using different CM tools, and the superiority of vibration analysis in comparison to other methods.

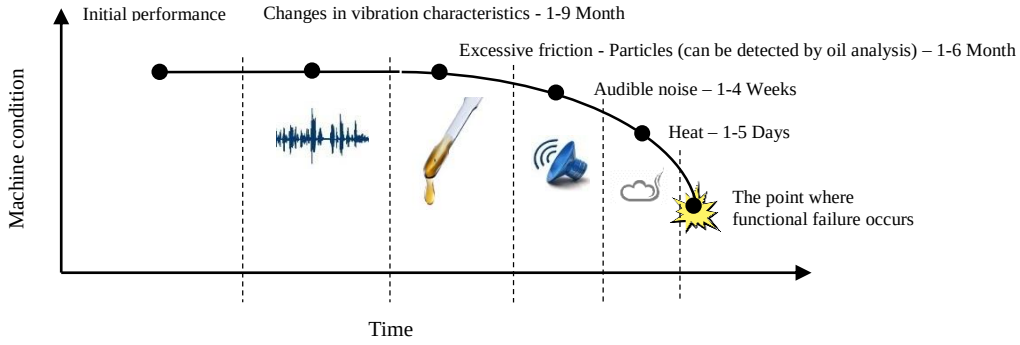

Figure 1.3. Monitoring tools based on P-F curve (Moubray, 1992)

A major advantage of vibration analysis is the capability to identify the existent of defects before they become too serious and cause unexpected breakdowns (Girdhar, 2004). Also vibration as a monitoring tool does not require any modification to the machine. Any machine running in good condition has a stable level of noise and vibration, which spectrum will change if any changes appear to machine condition (Heyns, 2008). Nandi

explained the advantages for this method regarding the sensors as non-destructive instruments. These sensors can provide continuous and full time monitoring capabilities, and are known as inexpensive monitoring instruments (Nandi et al., 2013).

Despite the advantages there are a few disadvantages associated with vibration analysis. Specifically on pumping systems that the recorded vibration signals are dependent on material and pump operating conditions. Also various types of vibration sensors with different characteristics exist and expertise is required to select the appropriate sensors and perform the analysis (Nandi et al., 2013).

1.3.3. Pumping Systems and Common Failure Modes

Pumps are devices that produce mechanical actions in order to move fluids or slurries. Mechanical pumps are presently applied in a comprehensive range of applications. There are different types of pumps that can operate in a variety of fields such as domestic or industrial applications with critical roles in operations. Failure occurrence may not only damage the system, but also can cause catastrophic failure in plants or affect the plant availability. In addition, defects may cause shock waves to the pump and lead to a reduction in the life cycle of all mechanical components.

Vibration Sources in Centrifugal Pumps

Vibration signals are often used to determine the condition and detect the mechanical faults in pumping systems. Vibration signatures include information related to amplitude, frequency and direction that provide crucial leads to diagnose the machine condition. It contains frequencies such as pumping frequencies related to the flow and recirculation, rotational speed, electrical excitation components and some mechanical failures like imbalance, misalignment, looseness, bearing defects, piping problems and resonance (Graney & Group, 2011).

A basic level of vibration in centrifugal pumps is expected with regard to the dynamic forces associated with mechanical and hydraulic sources. Potential failure and unusual running conditions could however cause higher levels of vibration and noise. All pumping systems vibrate due to excitation sources such as unbalanced rotors, turbulent flow, cavitation and wear of mechanical components and internal damages. Moreover, the magnitude of vibration increases rapidly if the frequency of vibration get close to the pump component resonance frequencies (Birajdar et al., 2009). Therefore, high levels of vibration indicates that there might be enough energy to lead to failure of component function. CTC Inc. mentions the common sources of vibration in centrifugal pumps

namely vane pass, flow recirculation, cavitation, unbalance, misalignment and bearing failures (Connection Technology Center Inc, 2012). Albraik et al. investigated the relations between pump performance characteristics such as head, flow rate and energy consumption, for the purpose of CM in pumping systems and the evaluation of performance. The results demonstrate that any defects on impeller can be obtained due to the effects on performance curve (Albraik et al., 2012).

Birajdar et al. have studied the sources of vibration in centrifugal pumps. This paper indicates three major sources that increase the vibration level in centrifugal pumps, namely peripheral (external), mechanical and hydraulic causes (Birajdar et al., 2009).

The peripheral causes are due to the external sources such as nearby machines, while the mechanical causes of vibrations include vibrating of the components due to the pressure variation in the liquid or air (or other pumping material) such as (Taneja, 2013):

- Mechanical imbalance of rotating components due to inexpert balancing, careless assembly or operational influence such as cavitation, erosion, corrosion, jammed parts, etc.
- Coupling excitation, especially when pump and motor are not aligned.
- Excitation from motor or gearing.
- Bent shaft
- Strain of the pipes
- Increase of the temperature in components
- Components in physical contacts
- Worn components
- Loose components
- Defected components
- Pump critical speed

On the other hand, a considerable amount of vibration in pumping systems is related to hydraulic excitations, which are generated from the flow interaction with the pump internal components. Taneja has listed the common hydraulic causes of vibrations as: "operating pump at other than best efficiency point (BEP), vaporization of the product, impeller vane running too close to the pump cutwater, internal recirculation, air in the system, turbulence in the system (non-laminar flow) and water hammer" (Taneja, 2013). Also, Birajdar et al. introduced hydraulic phenomenon in two groups, transient condition and non-stationary of flow, as described below (Birajdar et al., 2009):

Water hammer is an example of a transient condition that can be produced by opening and closing of valves to stop and start the pump. It causes sudden surges in pressure and can also cause impacts on the pump. The high levels of energy is then dissipated as vibration and noise. In addition, non-stationary flow can be caused by the secondary flow in the impeller due to rotation, number of blades, blade thickness, turbulence effects, pressure pulsation and cavitation. The number of blades and their thicknesses may lead to asymmetric flow with notches, and increase the vibration level.

Pressure pulsations are created by the interaction between fluctuating flow that leaves the impeller and impeller blades, at the blade passing frequency (BPF). The BPF is the number of blades N times the rpm (rotation speed) of impeller as presented in the equation below.

$$BPF = \frac{N \times rpm}{60} \tag{1.2}$$

Turbulence causes fluctuation in the dynamic pressure of the flow through the system and impacts the impeller by producing pulses. This phenomenon can generate vibration in rotating shafts. In addition, the existence of any restriction could cause turbulence and lead to vortices in the system. This generates vibration in a high frequency range that can excite resonant frequencies of other components. The vortex frequency is dependent on the flow velocity and the geometry of the restriction area. The frequency of turbulence in the system can be calculated using the equation below.

$$f = \frac{S_s \times V}{D} \tag{1.3}$$

where f is the vortex frequency (Hz), D is the dimension of the restriction area and S_s is the Strouhal number which describes oscillating flow mechanisms. The Strouhal number is a dimensionless parameter that varies between 0.2 and 0.5 (Girdhar, 2004).

Cavitation is a phenomenon that appears as high frequency and high energy components in vibration that can also be superimposed on to the BPF harmonics. Cavitation occurs when the fluid pressure drops below the vapour pressure. Since, gasses dissolve in liquid due to the inlet pressure of pumps, these gasses will escape from the liquid and appear as bubbles floating by reducing the inlet pressure. If the pressure drop reaches the vapour pressure of the liquid, then vapour bubbles will appear. As vapour bubbles travel through the pump into areas of increasing pressure, they collapse and release energy. The produced energy can cause damage to the internal components and affects the pump performance. Each explosion of bubbles causes an impact that generates high frequency vibration.

1.3.4. Vibration Analysis Techniques

Mechanical vibrations are most often measured by accelerometers, but velocity and displacement sensors are also available (Birajdar et al., 2009). Generally three quantities are used to describe vibration, namely displacement, velocity and acceleration. These quantities must capture the levels of vibration with respect to time, over a wide range of frequencies (Girdhar, 2004). Therefore, it is important to know which quantity is needed to be used to monitor the condition. Displacement and velocity can be converted by integrating the acceleration signal. Obtaining acceleration from the displacement signal through differentiation is generally risky because of the sensitivity of the differentiation process to noise in the signals (Heyns, 2008). Girdhar suggested a relationship between the use of these quantities, based on the vibration amplitude. He introduced the displacement measurement as a useful measurement unit for motions below 10 Hz which produces very little vibration in terms of acceleration and velocity, but relatively large vibrations in terms of displacement. Furthermore, for the high frequency range (over 1000 Hz) it is suggested that the acceleration yield more significant values than velocity or displacement, while velocity is a good indicator for the frequency range of 10 Hz to 1000 Hz (Girdhar, 2004).

On the other hand, it is also essential to choose a suitable analysis technique when using vibration as a CM tool. Several techniques are available and are explored in more details as follows.

1.3.4.1. Time Domain Analysis

This technique is known as a useful diagnosis process. It is a traditional way to extract significant information of signal behaviour over time. However signal evaluation by measuring the changes in vibration amplitude over time in raw signals, is complicated and

often does not reveal very sensitive information relevant to the actual condition. Hence, statistical methods have been in widespread use in time domain signals which provide vibration characteristics of the data (Sakthivel et al., 2010). Common statistical parameters are root mean square (RMS), impulse factor, shape factor, skewness, standard deviation, kurtosis and mean value.

RMS of a time history is a measure of the overall energy in vibration which is often used as a signal parameter for prognostic purposes and to trend data (Davies, 2015). The RMS value is known as an effective feature and an indication to identify the rotating machine condition. The RMS value including the energy of all elements, does however not necessarily help to identify defects in early stages (Heyns, 2008). Jantunen has mentioned series of tests that RMS value is evaluated through the performance of few other statistical parameters. The evaluation proved that RMS value may not be the best but it is one of the significant functioning parameters (Jantunen, 2002).

Mean, variance and skewness are the first three statistical moments of probability density distribution. Variance is a measure of signal points and shows how points are spread out. Also, the square root of variance is called standard deviation which is the amount of effective energy of the vibration (Sakthivel et al., 2010). The skewness value measures the level of asymmetry of a distribution, which the value of skewness for a normal distribution with symmetric data is zero.

The fourth statistical moment is known as kurtosis and is widely utilized in condition monitoring of rotating components. It is a dimensionless value that indicates the impulsive shape of a time signal. Without impulsive phenomena in time signal (for a normal distribution) the value of kurtosis is 3 while it can reach up to 50 with shocks (Lorenzo & Calabro, 2007).

Patel et al. introduced the equations of the most common statistical parameters (Patel et al., 2013). The corresponding equations are shown in table 1.1.

Table 1.1. Time domain features

Standard deviation	$\sqrt{\frac{\sum_{i=1}^{N}(X_i - X_M)^2}{N-1}}$	(1.4)

Root mean square	$\sqrt{\frac{\sum_{i=1}^{N}(X_i)^2}{N}}$	(1.5)
Crest factor	$\frac{PeakValue}{RMS}$	(1.6)
Skewness	$\frac{\sum_{i=1}^{N}(X_i-\bar{X})^3}{(N-1)S^3}$	(1.7)
Kurtosis	$\frac{\sum_{i=1}^{N}(X_i-\bar{X})^4}{(N-1)S^4}$	(1.8)
Impulse factor	$\frac{PeakValue}{(\sum_{i=1}^{N}(X_i))/N}$	(1.9)
Shape factor	$\frac{\sqrt{\sum_{i=1}^{N}(X_i)^2/N}}{(\sum_{i=1}^{N}(X_i))/N}$	(1.10)
Energy in time domain	$(\frac{\sum_{i=1}^{N}\sqrt{\lvert X_i\rvert}}{N})^2$	(1.11)
Lower bound	$\min(x)-\frac{1}{2}(\frac{\max(x)-\min(x)}{N-1})$	(1.12)
Upper bound	$\min(x)+\frac{1}{2}(\frac{\max(x)-\min(x)}{N-1})$	(1.13)
Entropy	$-\sum_{i=1}^{N}P_i\log(P_i)$	(1.14)
Central moments	$E(X-\mu)^k$	(1.15)
Signal distribution 1	$\frac{\sqrt{\sum_{i=1}^{N}(X_i)^2/N}}{\frac{1}{N}(\sum_{i=1}^{N}\lvert X_i\rvert)}$	(1.16)

Signal distribution 2 $$\frac{\max(x_i)}{\frac{1}{N}(\sum_{i=1}^{N}|X_i|)} \quad (1.17)$$

Deore and Khandekar have performed a time domain analysis on acceleration data of a 2 HP electric motor in order to extract information that helps to distinguish the signals from normal to faulty conditions. Five parameters were introduced as informative and primary statistical parameters, namely, peak value, RMS value, skewness, crest factor and kurtosis (Deore & Khandekar, 2014). Abdulkarem et al. investigated the effectiveness of the time domain statistical parameters in detection of impeller cracks. The results show that as the crack size increases, the value of time domain parameters increase (Abdulkarem et al., 2014). Sakthivel et al. applied a wide range of statistical parameters to a neural network for an online bearing condition monitoring. The authors suggested not to use all the parameters for online monitoring due to the correlation of features that may result ambiguous behaviour (Sakthivel et al., 2010). Heyns has introduced the time domain features that display good correlation and easy to be implemented which many condition monitoring systems rely on them, but also he has mentioned the sensitivity to disturbances as a drawback for time domain features. Therefore, other features from other domains are necessary to be used (Heyns, 2007).

1.3.4.2. Frequency Domain Analysis

Time domain vibration is mostly transformed to frequency domain and called spectral analysis. It can reveal information about signal that might not be apparent in the time domain. It also describes the signal power distribution over the frequency and gives us the essential information for condition monitoring. Randall suggests two main benefits of using the frequency analysis: Firstly, a rise in time domain features like RMS value is an indicator of having an internal disturbance but no indication about the causes of disturbance. Secondly, any minor changes or incipient failures can be identified in spectrum analysis (Randall, 1974).

Fourier transform (FT) is commonly used to deal with non-periodic signals that varies continuously over time (John & Putman, 2007). The most common approach to transform the data from time to frequency domain is known as the fast Fourier transform (FFT). This is a method of taking a time-varying signal and decompose it into components, each with an amplitude, a phase and a frequency (Shreve, 1995). Several studies are conducted with the intention to identify the fault initiation using frequency analysis. Yang et al. provided a review on vibration feature extraction techniques that are successfully implemented on rotating machinery data. The paper presents features from frequency analysis (FA) as

more sensitive, which can usually reveal information regarding the component defects better than the TDA features. The frequency characteristic like “resonance frequency components” or “defect frequency components” can be identified quickly (Yang et al., 2003). Nandi et al. have introduced parameters, namely arithmetic mean of a frequency spectrum, geometric mean and RMS amplitude of the frequency component, which provide a quick overview of the machine condition without specific diagnostic capability (Nandi et al., 2013).

Moreover, the frequency domain is commonly divided into three major frequency ranges which highlight specific faults. These are the low, medium and high frequency regions. Faults such as unbalance, misalignments, bent shaft, etc. reveal themselves as low frequency components around the shaft revolution speed (e.g. first harmonic). The second harmonic (2×rpm) indicates a bent shaft and misalignment. The appearance of such faults can therefore be detected in terms of changes in these frequency components. Some other indicators such as tooth meshing frequency in a gearbox (frequency corresponding to rotational speed multiplied by the number of teeth on the gear) and its harmonics can be identified in higher frequencies, and manifest themselves in the medium frequency range. Tooth cracks and wear influence the level of tooth meshing frequencies and its harmonics. Signals generated in rolling elements bearings are observed at even higher frequencies in the high frequency range that indicates defects like crack or corrosion on inner race, outer race or even on rolling elements. They create small impulses every time one of the rolling elements passes over it (Angelo, 1987).

Abdulkarem et al. used vane passing frequency and its harmonics as frequency domain indicators in crack diagnosis on a centrifugal pump impeller. The paper showed that the amplitudes at the relevant frequencies (VPF and its harmonics) increase as the crack size grows (Abdulkarem et al., 2014). Zhao et al. indicated pump rotational frequency, vane passing frequency and the second to tenth harmonics as frequencies to contain valuable information. This paper suggested using the amplitude ratios as features instead of directly using the frequency amplitudes, while some peaks are shown at fractional frequencies. Since the fractional frequencies become visible in frequency analysis of normal conditions, it is not clear if the fractional frequencies are due to the impeller defect (Zhao et al., 2010). Also, Liu and Ganeriwala have investigated vibration signatures due to cavitation in centrifugal pumps and the effects of cavitation on pump performance using spectrum analysis. From the observations it is deduced that cavitation appears at high frequencies and also that vibration along the axial direction is a better indication of abnormal conditions (Liu & Ganeriwala, 2012).

1.3.4.3. Time-Frequency Analysis

Rotating machines often do not operate under stationary conditions and the frequency composition is time varying most of the time. Fluctuating operations cause non-stationary conditions and changes in the signal information over time. Therefore, time-frequency analysis (TFA), which inspects vibration in the time and frequency domains, are introduced for non-stationary conditions. TFA includes signal processing methods in both time and frequency domains simultaneously. TFA aims to understand spectral evolution of a signal over time. This analysis technique is appropriate for non-stationary conditions where the spectral content varies with time.

TFA employs time-frequency distributions to display the energy density or intensity of a signal and reveal a more complete fault pattern. It intends to decompose a signal that contains several frequency ranges into different resolutions, and the reason for using this methodology is due to the changes of statistics of data over the operational period.

Short-time Fourier transform (STFT) or the power of STFT (spectrogram), Wigner–Ville distribution and wavelet analysis are the most common time-frequency representations (Jardine et al., 2005). Wang et al. investigated the performance of common TFA methods in an intelligent diagnostic procedure for an accelerating vehicle noise in order to identify the various failure modes. The comparison results of five TFA techniques show that wavelet analysis techniques render more suitable information regarding the operating condition of a system (Xing et al., 2015). Some common TFA techniques are explained in more detail in the following sections.

Short time Fourier transform

Short-time Fourier transform (STFT) is a Fourier based transform by a fixed-sized, moving window to a signal. STFT determines the frequency and phase content of signals as they change over time. Implementing the discrete Fourier transform (DFT) over a long window under non-stationary conditions does not reveal transitions in spectral content, therefore it is needed to implement it over short periods of time to overcome this problem.

The main STFT steps are (i) Define a window function of limited length, (ii) Define the amount of overlap between windows, (ii) Generate windowed segments (multiply signal by windowing function), (iv) Compute the FT of the windowed segment and save results, (v) Slide the window to the right until the window achieves to the end of the signal and reveal the Fourier spectrum on each segment. (vi) Finally plot the changing spectra as a function of time.

$$STFT(t',u) = \int [f(t).W(t-t')].e^{-j2\Pi ut}dt \quad (1.18)$$

where STFT of $f(t)$ computed for each window centered at $t = t'$, t' is time parameter, u is frequency parameter, $f(t)$ represents time domain signal to be analysed and W is the window function centered at $(t-t')$.

One of the disadvantages of the STFT is that the resolution is dependent on the window length. The length of the windowing function determines whether there is a good frequency or a good time domain resolution. In other words: A short window performs a good time resolution but poor frequency resolution. On the other hand, a longer window length gives more uncertainty on the instant that the signal changes. Jardine et al. introduced STFT as a method that can only be used for non-stationary conditions when the the dynamics change relatively slowly (Jardine et al., 2005).

Wigner-Ville Distribution (WVD)

The Wigner–Ville distribution (WVD) is a bilinear transform technique. Since WVD is not based on dividing signals in to various sections, it can overcome the difficulties of time-frequency resolution (Jardine et al., 2005). Baydar and Ball mentioned the interference terms and its difficulty to interpret the time-frequency representation as drawback of the WVD. Also a smoothed version of the WVD is presented to overcome this problem and reduce the presence of interference components (Baydar & Ball, 2001).

Wavelet Transform

Like FA, wavelet analysis expands the signals in terms of wavelets that are produced through a set of scale and translation of a wavelet called mother wavelet (Lee & Yamamoto, 1994). WT is introduced as an effective approach that deals with non-stationary signals such as vibration signals (Chebil et al., 2009).

From a historical point of view, Alfred Haar was the first person who introduced wavelets and developed the Haar wavelet. Later on Paul Levy (1930) found out that the Haar basis function performs better than the Fourier functions. The major advancement in the field of wavelet research is due to Jean Morlet (1970), who improved the method of scaling and shifting of the wavelet functions. He worked on the idea of transforming the signals using wavelets without any change in information with the help of Alex Grossmann, which led to proposing the continuous wavelet transform (Gao & Yan, 2011).

Unlike a time-frequency distribution that includes a fixed time and frequency resolution, WT represents a time scale of a signal. Wavelet analysis has improved in the recent decade and has broad applications nowadays (Jardine et al., 2005). WT provides scale-varying functions for the analysis of different frequency component in a signal. WT uses non-stationary functions (wavelets) with variable window sizes, which can be moved along signals to generate an individual time-frequency map.

A number of wavelet transform methods have been introduced including the continuous wavelet transform (CWT), the discrete wavelet transform (DWT) and the wavelet packet transform. Sifuzzaman et al. listed a wide range of applications that WT can effectively be used, namely (Sifuzzaman et al., 2009):

- "Signal analysis
- Data compression
- Image denoising
- Verification of fingerprint
- Biology for cell membrane recognition, to distinguish the normal from the pathological membranes
- Analysis of DNA
- Blood-pressure and heart rate analyses
- Finance, for detecting the properties of quick variation of values
- In internet traffic description, for designing the services size
- Industrial supervision of gear-wheel
- Speech recognition
- Computer graphics and multifractal analysis"

The continuous wavelet transform (CWT) is given by:

$$X_{WT}(\tau, s) = \frac{1}{\sqrt{s}} \int_{-\infty}^{+\infty} X(t) \psi * (\frac{t-\tau}{s}) dt \tag{1.19}$$

where τ moves the scaled wavelet over the time axis, s denotes the scaling parameter that defines the resolution of time and frequency of the mother wavelet $\psi(t-\tau/s)$. Also $\psi *$ denotes the complex conjugation of the mother wavelet (Gao & Yan, 2011).

CWT consists of three main steps: (i) Comparison of the selected wavelet with a segment at the initial signal and compute the correlation parameter C. (ii) Moving the wavelet along the signal and repeat the previous step until the signal is covered. (iii) Scale (stretch) the wavelet and repeat the previous steps (one and two). (iv) Repeat steps 1 to 3 for all scales (Berkouk & Sadmi, 2014). The shifting and scaling process of the mother wavelet in CWT is depicted in figure 1.4.

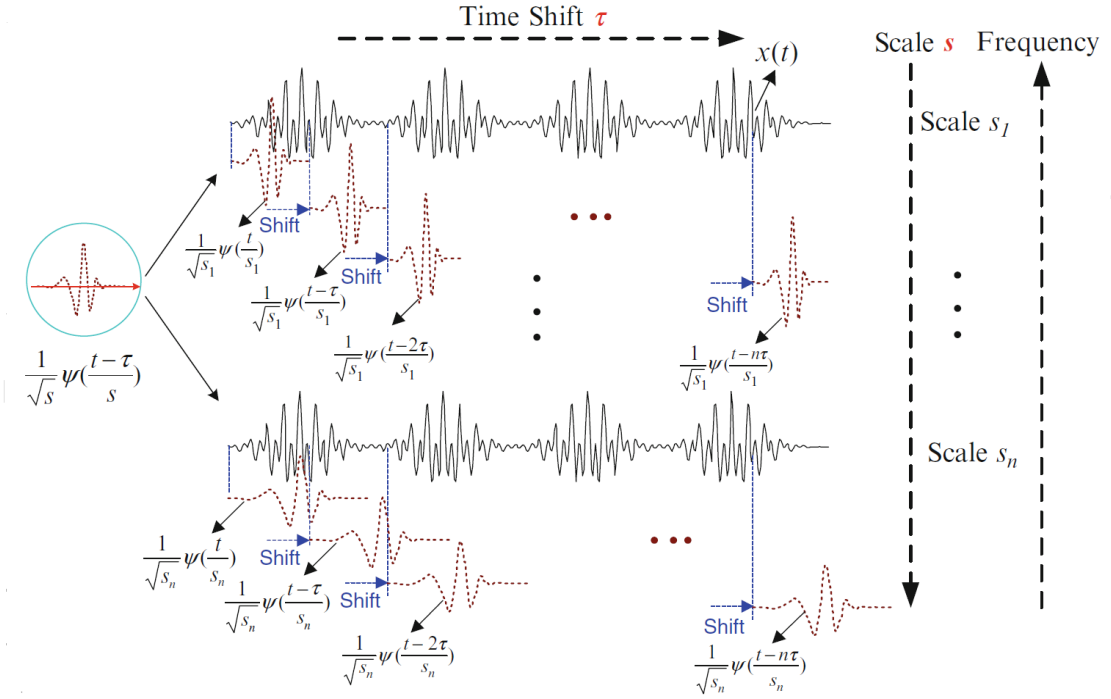

Figure 1.4. Illustration of CWT (Gao & Yan 2011)

Discrete Wavelet Transform

The discrete wavelet transform (DWT) is a form of wavelet transform that uses a discrete series of wavelet scales and dilations based on power of two rather than each set of scale and dilations in CWT. In other words this method breaks down the signal into orthogonal series of wavelets (Klapetek et al., 2015).

$$X_{DWT}(m,n) = \langle \psi_{m,n}, f \rangle = \int_{-\infty}^{+\infty} \psi_{m,n}(t) f(t) dt \tag{1.20}$$

For a given mother wavelet:

$$\psi_{m,n}(t) = \frac{1}{\sqrt{2^m}} \psi\left(\frac{t - n2^m}{2^m}\right) \tag{1.21}$$

where $\psi_{m,n}(t)$ is called the DWT basis. The signal is analysed by DWT over various frequency ranges and resolutions by breaking down the signal into series of information called approximation and detail (Zhang et al., 2010). The DWT decomposition process can be illustrated as a tree including two complementary filters which decompose the vibration signal into low and high frequency components. It can be repeated through other levels to decompose the low frequency components, since the high frequency components are not decomposed further. (Mesbah et al., 2003). The structure of DWT is shown in the figure below.

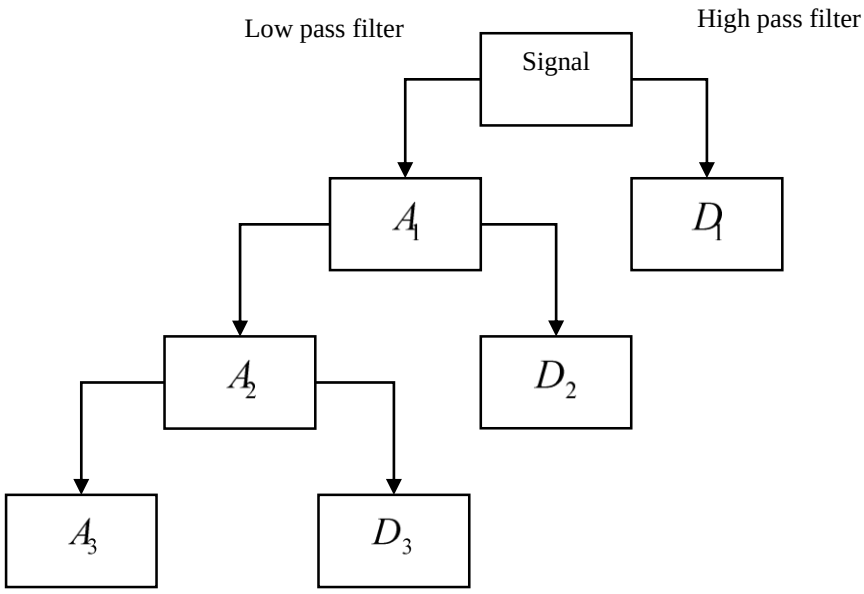

Figure 1.5. Discrete wavelet decomposition diagram

In contrast with CWT which represents more information and requires a very large computational time, DWT reveals efficient details with fewer parameters and less computational time (Chebil et al., 2009). However, one of the significant drawbacks of the DWT is the decomposition process. In this process only the approximation coefficients are decomposed to next level and can cause improper frequency resolution. Hence, wavelet packet transform (WPT) was introduced to alleviate this weakness by decomposing both low and high frequency components simultaneously at each level. Figure 1.6 shows the structure of WPT decomposition.

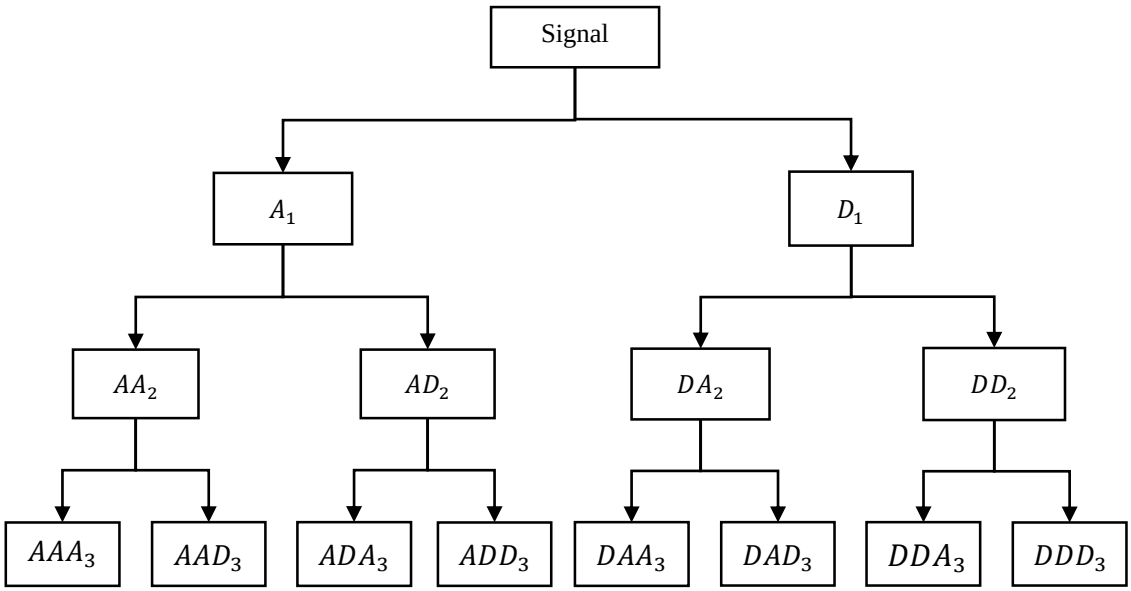

Figure 1.6. Wavelet packet decomposition diagram

Jardine et al. discussed one main advantage of the WPT as its capability to present high time and frequency resolutions for non-stationary signals containing a large number of frequency range. It is also capable to alleviate the noise in signals (Jardine et al., 2005).

Wavelet based analysis methods have been successfully applied to process signals in machine fault diagnosis. In the recent decade, several researches on WT have been carried out to examine signals where the FFT was not efficient. Toth compared the performance of Meyer and Morlet wavelets in WPT for bearing fault diagnosis. The Morlet wavelet was found to be superior to Meyer in representing transient signals of bearing vibration (Toth, 2013). Kankar et al. used CWT as feature extraction methods and classified them using machine learning methods. Comparison of two wavelet selection methods are provided to choose the superior wavelet for feature extraction, namely maximum energy to Shannon entropy ratio and the maximum relative wavelet energy. It is concluded that wavelets selected using maximum energy to Shannon entropy ratio criterion (Meyer wavelet) provide a better classification result (Kankar et al., 2011). Loughlin et al. introduced a group of time- frequency parameters as features and applied these parameters to helicopter test data for fault diagnosis. These conditional parameters are mean, median and mode frequencies at a given time. This research showed the capability of these features to characterize the faults which can differentiate between different fault classes (Loughlin et al., 2000).

According to Lauro et al. CWT among different wavelet features in condition monitoring, is recognized as an effective tool in both stationary and non-stationary conditions, however they include much redundant information in comparison to DWT, which has a fast algorithm based on conjugate quadratic filters (Lauro et al., 2014). Chen et al. investigated the WPT method on piston fault detection in water hydraulic motors. In this paper the impulsive energy of the vibration is extracted from the reconstructed signals after three level of decomposition. The results proved the ability of WPT to detect the piston defects in the water hydraulic motor (Chen et al., 2008).

Moreover, energy entropy is introduced as a good indicator that presents the behaviour of non-stationary vibration of frequency subbands. Zhang et al. introduced the wavelet packet based energy as a reliable method that is more appropriate to be used in fault detection in comparison to other methods, which can presents the signal energy in various frequency bands (Zhang et al., 2010). Therefore, the energy entropy of different nodes of the signals after decomposition can be useful in revealing convenient information regarding the impeller condition for the purpose of this study.

There are several definitions of energy entropy, Zhang et al. introduced the energy entropy and the Shannon entropy. The wavelet packet energy entropy Ent_n at a specified node n in the wavelet decomposition tree can be computed using the equation below, where $C_{n,j}$ presents the wavelet packet coefficients at time j and node n.

(Zhang et al., 2010):

$$Ent_n = \sum_n |C_{n,j}|^2 \tag{1.22}$$

In addition, log-energy entropy is also introduced as useful parameter, the following equation presents log-energy entropy of a signal $Entl_n$:

$$Entl_n = \sum_j \log(C_{n,j}^2) \tag{1.23}$$

1.3.5. Intelligent Systems and Failure Prognostic Tools

Intelligent learning systems iteratively learn patterns from features and can understand how to implement significant tasks by building analytical models from samples. In the past recent years the use of intelligent systems has rapidly increased. Intelligent learning systems are used in "web searches, spam filters, ad placement, credit scoring, fraud detection, stock trading, drug design and many other applications". Many various types of intelligent systems are existed, but the most well-known and widely used is classification (Domingos, 2012). A classifier is a system that assigns a group of feature values and outputs a value as the predicted class. Domingos presented three main components for an efficient learning process:

$$\text{Learning} = \text{Representation} + \text{Evaluation} + \text{Optimization}$$

where the "representation" step consists of the input data. The classifier includes the process and selection of the most appropriate one for the problem in order to get the best result. An "evaluation function" is needed to distinguish how effective the performance of a classifier is. "Optimization" is a method to search among the classifiers for the highest performance rate (Domingos, 2012).

There are different ways for an algorithm to model a problem based on input information. It is popular in machine learning and the artificial intelligence field to consider the learning methods that an algorithm can adopt. There are only a few main learning methods or learning models, namely supervised learning (SL), unsupervised learning (USL), semi-supervised learning (SSL) and reinforcement learning.

Supervised learning is a model that is created through a training process using labelled data (inputs and outputs are available), where it is required to make predictions and apply corrections when the predictions are wrong. The training process continues until the model achieves an acceptable level of accuracy on the training data. However, in the unsupervised learning method, the input data is not labelled and does not have a known output. This model is prepared by clustering the given input data in classes based on their properties.

Semi-supervised learning algorithm is a model, in which the input data is a mixture of labelled and unlabelled examples. This model must learn the patterns to cluster the data as well as make predictions.

On the other hand, reinforcement learning is a model in which the input data is provided from an environment and the model must respond and react. Feedback is provided not from of a teaching process as in supervised learning, but as penalty and reward in the environment. Example problems are systems and robot control (Brownlee, 2013). It allows the model to automatically predict the ideal output within a specific background in order to maximize the performance.

The fault diagnosis task comprises the detection of detailed fault categories such as the size and location of defects. On the other hand, diagnosis of machine condition typically needs technical experience and skills due to having several components and complexity of equipment. Also it requires specific expert with the appropriate background and maintenance knowledge regarding to the machine structure and general concepts of fault detection, which the expert might not be available. Hence, some automatic fault diagnosis methods are introduced to speed up the detection process and to make decisions about the machine conditions, such as artificial neural networks (ANN), expert systems, fuzzy logic, support vector machine (SVM), nearest neighbour algorithms, and model-based methods (El-Thalji & Jantunen, 2015). Due to the intention of this study which is the evaluation of ANN methodology in impeller fault detection, it is further explored in more details as follows.

Artificial Neural Networks

An artificial neural network (ANN) is an effective processing tool for nonlinear problems that is inspired by the biological neural networks, such as the data processing mechanism in brain. An ANN is designed for specific purposes like pattern recognition or data classification through learning procedures in order to achieve fault diagnosis. Learning in biological neural networks include adjustments to the synaptic links, where this is the same process for an ANNs as well (Maind & Wankar, 2014). ANNs are the most extensively used intelligent systems in different fields for a number of advantages such as high learning speeds, better approximation ability and stronger tolerance to input noise (Qu et al., 2015). ANN applications use a simple multi-layer perceptron (MLP) as the network common architecture.

The operation in this type of MLP network is based on two stages, feedforward and back-propagation, respectively. The network is propagated by inputs and results to an output. In the second stage, a comparison is provided between the output and the expected value for the output. Subsequently, the error value corresponding to each output node is computed in order to be transmitted backwards and adjust the network weights. A typical MLP network architecture is depicted in figure 1.7. Each layer is formed by a number of neurons, where each neuron includes a sum of inputs x. Afterwards, the neuron values are normalized to a specific range by passing through an appropriate activation function f. The output of the network y is described in a matrix form as the equation 1.24 (Unal et al., 2014).

$$y = f^2(w^1 f^1(w^1 x + b^1) + f^2) \tag{1.24}$$

where w denotes the weight matrix, b is the bias vector, and f is the activation function. f^1 is a hyperbolic tangent sigmoid function and f^2 a linear function. Also, $w_{i,j}$ presents weight between i^{th} output and j^{th} input layer.

The back-propagation in ANN is considered as a simple method in mapping the non-linear relationship between inputs and the outputs of networks, and provides supervised training of MLP networks. It generalizes the least squares algorithm and updates the network weights in order to reduce the mean square error e described in the equation below:

$$e = \frac{1}{2}\sum_{i=1}^{N}(trg^i - y^i)^2 \tag{1.25}$$

where y is the network output, trg is the target, N is the sample size and i is the sample number (Unal et al., 2014).

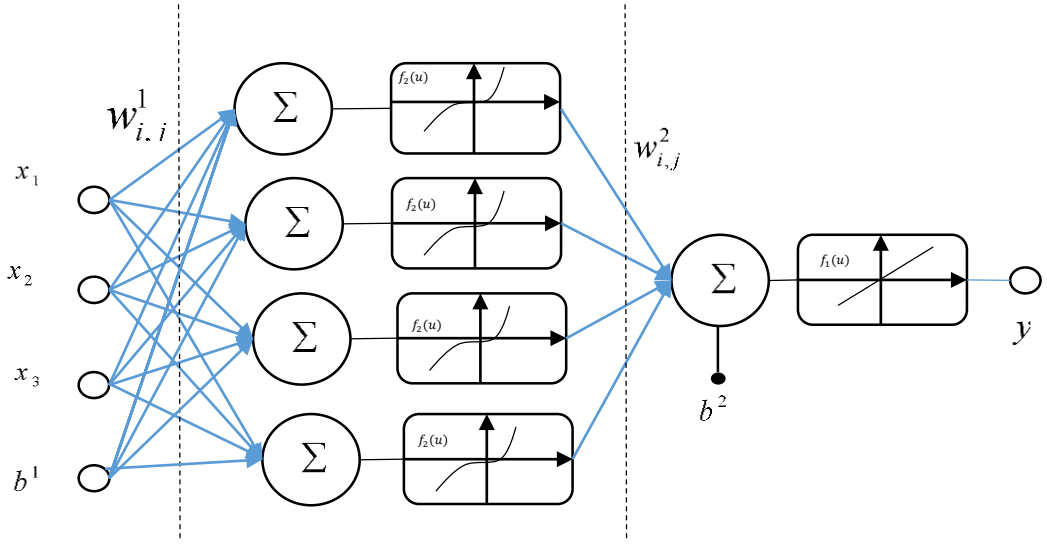

Figure 1.7. Neural network architecture

The back propagation algorithm applies a gradient descent technique on the error considered as function of the weights. There will be a gradient for weights that aid in finding the desired value for weight in each neuron to minimize the error by moving the weight along the negative gradient of performance function. The back propagation algorithms consist of two main steps, namely training and testing. In training step the network is given the sample features and the correct classification to define the network architecture. Then the network will be tested in the second step using new data sets against the correct output to evaluate the accuracy of network.

Moreover, sums of weighted inputs of nodes are needed to pass through a non-linear function known as an activation function in order to calculate threshold value and yielding the nodes outputs. There are a number of popular activation functions for ANNs. Common activation functions are linear functions, threshold functions, unipolar sigmoid function and bipolar sigmoid functions (Karlik & Olgac, 2010). In this study a unipolar sigmoid function as a differentiable function, will be used for hidden layer output (equation 1.26).

$$y_j = \frac{1}{1+e^{-x}} \tag{1.26}$$

This function is a common function in neural networks and has particular advantages for networks trained by backpropagation algorithms, due to its simplicity to differentiate which can strongly reduce the computation time in training (Karlik & Olgac, 2010), it is suitable for pattern recognition networks with output values between 0 and 1.

There are important aspects to consider in designing a reliable network architecture, such as the number of hidden nodes and hidden layers. The number of nodes in the processing layer (hidden) has a great impact on the accuracy of an ANN performance. A large number of input nodes in hidden layer gives the ability to map complex data sets, but it can also lead to an under-trained or an over-trained network. Under-training occurs when hidden nodes are not sufficient enough to map the complex data sets. On the other hand, if the number nodes in hidden layer are more than required, over training can occurs and training time will significantly increases. Hence, both conditions cannot present patterns regarding the complexity of data sets. The number of nodes in a hidden layer is generally difficult to define. It can be estimated by the empirical equation 1.27 (Xing et al., 2015).

$$L = \sqrt{M + N} + \alpha \tag{1.27}$$

where M and N denote the node number in input and output layer and α is a constant value between 1 and 10.

ANNs have been utilized as intelligent fault diagnosis of rotary machinery in order to classify conditions based on feature patterns extracted from experimental vibration signals (Samanta, 2004). Zouari and Menad presented a fault diagnosis procedure using an ANN. They investigated the ability of ANNs to detect and classify some specific faults such as "partial flow rates, loosening of rear pump attachments, misalignment, cavitation and air injection on the inlet". The features are computed from the time domain and frequency spectrum respectively (Zouari & Menad, 2005). Maind and Wankar have reviewed the applications and advantages of ANNs. They mentioned some advantages for ANN systems such as: pattern extraction and trend detection from complex data, the ability to learn how to predict the output classes based on the input features (adaptive learning), generating its own prediction of the information that receives as inputs during learning period (self-organisation) (Maind & Wankar, 2014).

Xing et al. presented a method which combines wavelet packet transform and artificial neural network in order to analyse the quality of sounds (Xing et al., 2015). A WPT with 21 critical bands is utilized to extract sound features, a three-layer ANN model with back-propagation is used for sound quality recognition. The WPT–ANN is also used on vehicle noises under various conditions to illustrate its effectiveness in showing a time varying energy pattern. The extracted features were used as the ANN input, and the calculated loudness and sharpness from Zwicker-model (Zwicker developed a method for the computation of noise levels, ISO 532B) used as ANN output.

Samanta compared the ANN performance with SVM in terms of accuracy of results and training time. He used the time domain signal under different operating speeds and bearing conditions for feature extraction in order to train both classifiers. Also a genetic algorithm (GA) is applied in feature selection and network optimization. In addition, he has mentioned over-fitting of training data as a drawback for ANNs, which is due to the optimisation algorithms used in ANNs for selection of parameters (Samanta, 2004).

1.4. Scope

The required performance of assets has received more attention during recent years. Nowadays business policies of organizations are structured to achieve top performance in order to maximize their capabilities, operations and customer satisfaction. Since, the majority of total life cycle costs is derived from operation and maintenance, fault detection can assist during the operational period and keep assets at the required performance levels. It causes a reduction in unscheduled shutdowns and maintenance costs by provision of preventive maintenance, optimal replacement decisions and scheduled shutdowns that allow maintenance teams to order parts in advance, schedule manpower, or plan other repairs during the downtime.

As mentioned previously, a successful condition monitoring system helps to detect the potential failures before functional failures occur. An efficient CM includes a continuous periodic monitoring, data processing and diagnosis that leads to updated machine condition information. These concepts are known as “diagnosis and prognosis procedures”. The role of effective condition monitoring is undeniable in maintenance strategies. Various monitoring methods are used to identify failure signs in equipment during the operation period to monitor machine health state.

This dissertation proposes an investigation of the neural networks methodology in condition monitoring of centrifugal pump impeller under fluctuating flow conditions using vibration signals. Impellers are perhaps the most critical components in pumps and their condition is usually important to satisfy the required performance. Therefore, there is a great need for a monitoring tool to identify the health state of impeller conditions. Generally, machine condition monitoring determines the component's health states based on data collection, processing and prediction in order to identify the sources of problems. Figure 1.8 depicts the flowchart of fault diagnosis procedure.

For this research a pump system was designed and constructed to simulate different types of defects in a pump impeller such as cavitation, unbalance and cracks. A small centrifugal pump was utilized to simulate common failure and the corresponding vibration was

monitored. Information regard to the impeller condition was collected from acceleration measurements of the vibration in three dimensional coordinate axes (triaxial accelerometer was used), in order to provide more reliable data and observe vibration intensity in all three axes.

Signal processing is performed in time, frequency and time-frequency domains respectively. The time domain signals are evaluated by statistical parameters, namely RMS, peak value, crest factor, kurtosis, skewness, standard deviation, impulse factor, shape factor and signal energy, in order to observe the influence of defects on vibration and extract the relevant indicators. In addition, results of the frequency analyses are used to interpret the effect of defects on the frequency spectrum. Although an attempt is made to illustrate the possibilities and advantages of utilizing a time-frequency analysis. Wavelet packet analysis is therefore applied to the vibration signal to extract the effective features due to flow fluctuation.

Finally, an investigation of the neural network toolbox in Matlab R2015a is provided. The system is used to extract desired fault features and measure the effects of fault vibration characteristics on pump performance. These results are used to design an artificial neural network capable of impeller fault detection in any pump from measured on-line vibration signals. The flowchart below gives a basic run through of the proposed methodology, beginning with the unprocessed time domain vibration signal.

1.5. Report Layout

This dissertation is structured under the following chapters:

Chapter two describes development of the experimental rig. A review of the design of the pumping system, including the data acquisitioning system, the required equipment and system characteristics is presented. Also common types of damage in centrifugal pump impellers and the relevant severity of damage and their influence on pump vibration are discussed.

Chapter three presents signal processing techniques, feature detection, selection, extraction and classification. The vibration signals of the simulated conditions are analysed in three domains, namely time, frequency and time-frequency domains. Signal characteristics are extracted from each domain under the various flow rates, in order to evaluate the signal characteristics over flow fluctuation. The intention of this chapter is to select the appropriate parameters and eliminate the redundancies.

Chapter four presents a review of the fundamentals of artificial neural networks as machine learning systems, such as number of nodes in hidden layer, transfer functions and training algorithms. Based on data features extracted from simulated signals in chapter three, ANNs capable of pattern recognition are trained. Furthermore, comparison of ANNs performances are provided to evaluate the effectiveness of signal processing methods on the output of each trained network. Finally, each developed ANN is evaluated by new testing data sets.

Chapter five presents a discussion of the results of the proposed methodology when applied to the generated signals from pumping system. Also, some suggestions are made in chapter six in order to extend the present research.

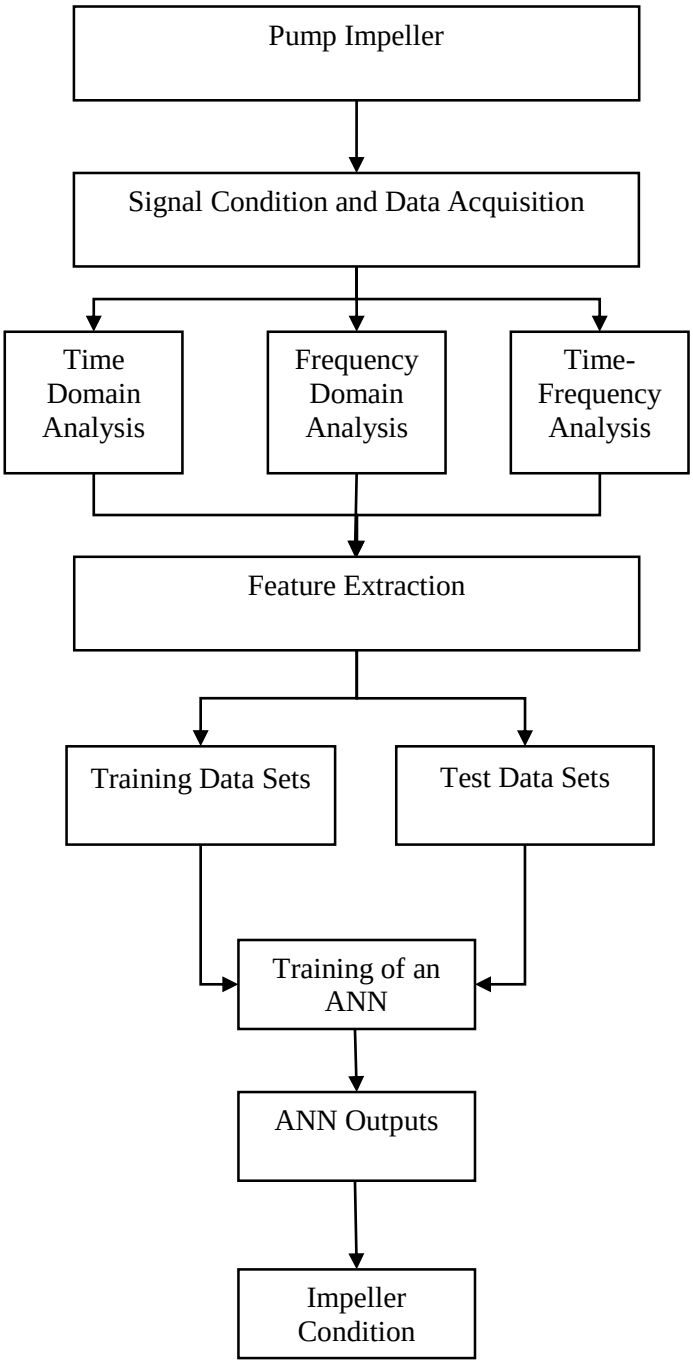

Figure 1.8. Flowchart of fault diagnosis procedure

2. Experimental Development

2.1. Introduction and Overview

The aim of this chapter is to review the system design for the purpose of condition monitoring studies using vibration characteristics of a pumping system. A test setup that contains a centrifugal pump and a closed loop piping system for water flow is designed.

According to the general approach discussed in chapter one, the present chapter concerns developments on the experimental setup. The important aspects of the setup and review in designing a pumping system are presented. Moreover, data acquisition, experimental equipment and the required procedures on this research are illustrated in detail. This chapter covers two different impeller damage scenarios, cracked and imbalance, respectively. In addition, effects of cavitation on impeller performance are of concern due to the fluctuating flow conditions. Each type of damage comprises three different sizes indicating the damage severity. Analysis of vibration signals are studied in order to determine the condition of impeller and severity of defects. Finally the experiment is conducted on a small CM 50 Pentax centrifugal pump.

2.2. Experimental Setup

Data for this research is obtained from an experimental setup that contains a centrifugal pump and closed loop water piping system for water circulation. A single suction pump with top discharge, operating at 2700 rpm, with a single phase electrical motor is used in this work. The pump is a CM-50 Pentax series single impeller centrifugal pump with the following construction features: Cast iron body and motor bracket, Noryl impeller, ceramic-graphite mechanical seal, allowance temperature 0 to 90 for brass impellers and 0-50 Celsius for Noryl impellers, which can deliver water at a rate of up to 90 l/min and at a head of up to 21m.

The closed loop water system is shown in figure 2.1. It is designed with the shortest possible pipe line in order to reduce the friction pressure loss.

`

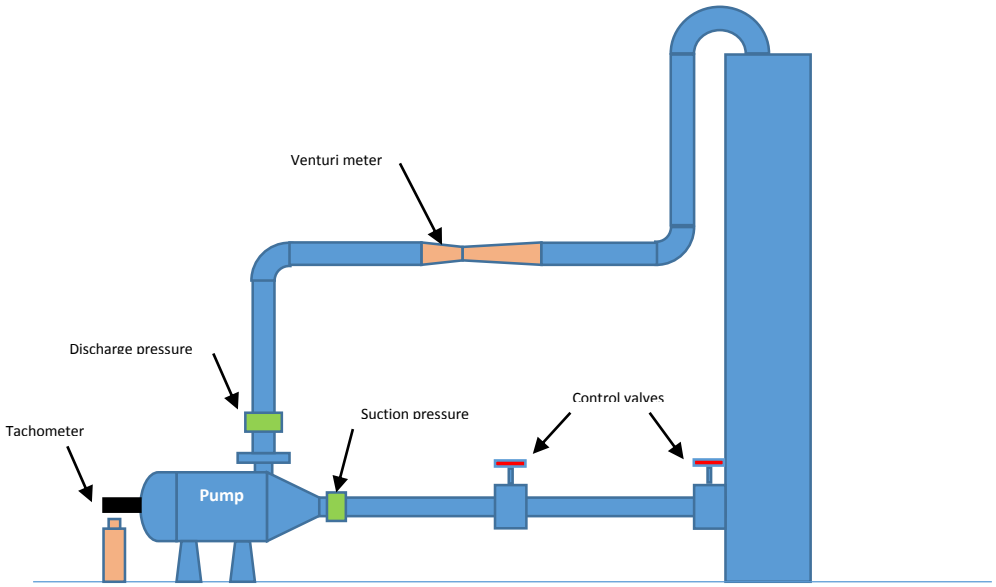

Figure 2.1. The schematic diagram of the experimental setup

Two flow valves are designed to be installed in the inlet line of pump and discharge of the tank in order to control and modify flow rate in the suction pipe as well as water height in the tank. In addition, two pressure gauges are installed to measure the suction and discharge pressure.

The tank size is chosen to allow the maximum allowable flow rate with the height of 4m to provide the required inlet pressure in the system. The outlet flow of the tank in terms of velocity and volume can be calculated as shown in figure 2.2.

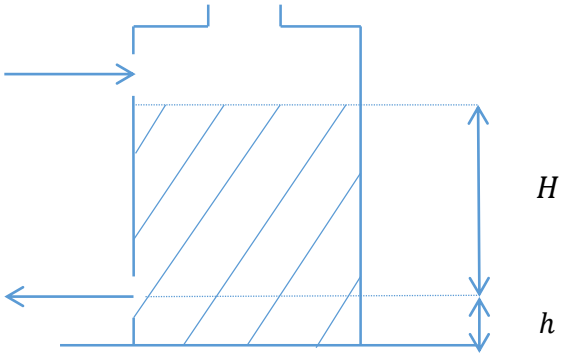

Figure 2.2. A Schematic water tank

Fluid flows from the tank through an orifice close to the bottom, where the Bernoulli equation can be adapted to obtain the tank outlet parameters as below (White, 2011):

The velocity V of fluid flowing past a point per unit time [m/s], which depends on the depth of fluid h, acceleration of gravity g and velocity coefficient Cv, can be calculated using equation 2.1.

$$V = C_d \sqrt{2gh} \tag{2.1}$$

Moreover, the volumetric flowrate Q of fluid flowing past a point per unit time [m^3/s] depends on the velocity of fluid and the cross-sectional area of orifice.

$$Q = C_d A \sqrt{2gh} \tag{2.2}$$

Where the discharge coefficient C_d is a dimensionless number representing the ratio of actual discharge to the ideal discharge, and also depends on the velocity coefficient C_v, (0.97 for water) and the orifice contraction coefficient C_c, (sharp edge orifice 0.61, well rounded orifice 0.97).

$$C_d = C_c C_v \tag{2.3}$$

Therefore, for the specified parameters of the designed tank on this study with the height of 4m and the outlet orifice diameter of 0.02m, considering the contraction coefficient $(C_c = 0.75)$ and the velocity coefficient of water $(C_v = 0.97)$, the volume and velocity for the water entering to the system can be achieved as table 2.1.

Table 2.1.Estimation of the maximum outlet flow rate for the designed tank

Parameter	Estimation
Discharge coefficient (C_d)	0.72
Velocity (V)	6.37 m/s
Volumetric flowrate (Q)	0.002 m^3/s = 120 l/min

The above results show that the flow rate at the outlet of tank is much higher than the required flow rate for the specified pump in this study which operates in flow range of 20 to 90 l/min.

2.3. Performance Measurement

2.3.1. Pressure Measurement

In order to monitor and control the system, measurements are performed after setting up the pumping system. The system pressure and effects on pump performance are measured using pressure gauges in the suction section as well as discharge section. Pump relevant head h can be determined using the measured pressure by equation 2.4.

$$h = \frac{\alpha \times P}{SG} or \frac{P}{\rho \times g} \tag{2.4}$$

Where P is the discharge pumping pressure in the unit of [Bar], SG is specific gravity (water = 1) and α is a constant factor which is calculated using the equation above to be 0.0001037 for water.

In addition, Tacket et al. introduced parameters such as actual suction pipe length, flow velocity in suction line and the properties of fluid as key factors influencing the suction conditions. If sufficient energy is not available, problems such as cavitation and vibration will appear in the system. It is therefore critical to supply the required pressure at the pump inlet in order to overcome these problems. Hence, the equation 2.5 is being introduced to determine the essential available head H_a in [m] to produce the required acceleration (H.Tackett et al., 2008).

$$H_a = \frac{LVNC}{gk} \tag{2.5}$$

where L is the actual suction pipe length [m], V presents the velocity of flow, N is pump speed (rpm), C is pump constant factor (0.115), g is the acceleration of gravity (9.81 m/s^2) and k is the liquid factor (1.4 for water).

Therefore, the required head at the inlet of pump using the equation above considering pump speed at a constant speed of 2700 rpm is 3.23m, which due to height of the designed tank (4m), the required pressure will be provided at the inlet of the pump.

Moreover, as flow rate changes, the pump output pressure gives the ability to check the discharge head. It is also applicable to control if the pump operates in the expected head according to the standard performance curve. The discharge head for the CM50 Pentax pump on this study is estimated to vary between 20.1m and 12m. Pump specifications and

the performance curve obtained from Pentax product catalogue, are presented in figures 2.3 and 2.4.

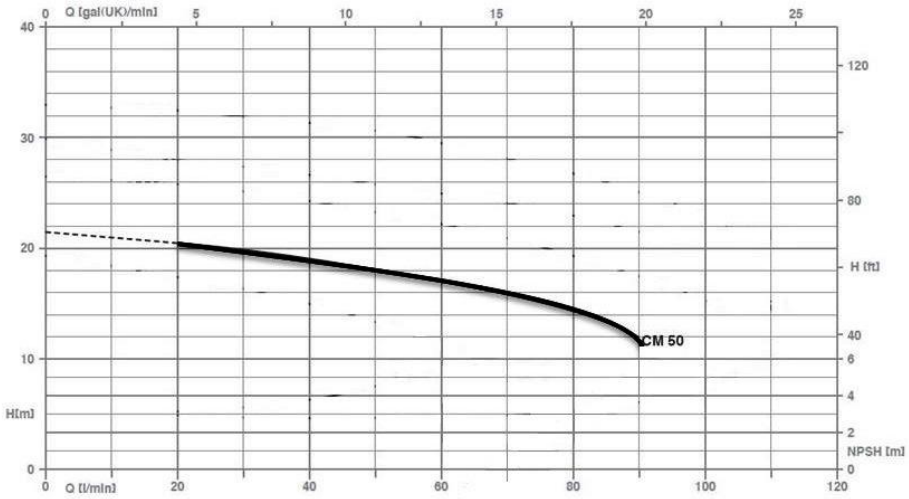

Figure 2.3. Variation of CM50 Pentax pump head against flow rate (Pentax Co. 2013)

TYPE		P2		P1 (kW)		AMPERE		Q (m³/h - l/min)						
1~	3~					1~	3~	0	1,2	2,4	3,6	4,2	4,8	5,4
								0	20	40	60	70	80	90
		(HP)	(kW)	1~	3~	1x230 V 50 Hz	3x400 V 50 Hz	H (m)						
CM 45	CMT 45	0,4	0,3	0,51	0,56	2,3	1	19,3	17,4	15	11,3	8,9	-	-
CM 50	CMT 50	0,5	0,37	0,59	0,65	2,8	1,1	21,5	20,5	19	17	15,8	15	12
CM 75	CMT 75	0,8	0,59	0,9	0,94	4,5	1,7	26,5	25,8	24,5	22,2	20,9	19,5	17,5
CM 100 V	-	1	0,74	1,05	-	4,6	-	30	28	26,6	25	24,1	23	21,5
CM 100	CMT 100	1	0,74	1,16	1,17	5,7	2	33	32,5	31,5	29,6	28,3	26,8	25,2

Figure 2.4. CM50 Pentax specification, head variation vs flow variation (Pentax Co. 2013)

2.3.2. Flow Measurement

Positive displacement flow meters measure a fixed volume of fluid and count the number of times that the volume will fills the measurement volume. On the other hand, the other methods are based on force measurement that are produced by the movement of fluid and are known as pressure based meters.

Several methods exist in order to measure the flow rate and are based on Bernoulli's principle. Venturi and Orifice meters are the most common flow meters that rely on differential pressure measurement of the fluid flowing through the pipe. In this study a venturi meter as a reliable differential head meter was designed to measure the system flow rate.

The venturi meter was designed based on standard ISO 5167 (figure 2.5). The exact dimensions used may be found from a SolidWorks drawing given in Appendix A. According to ISO 5167 the venturi walls should converge at about 20° and diverge on the downstream side at about 5 to 7°. In addition, the flow rate Q_v can be calculated as equation 2.6.(Gill et al., 2011).

$$Q_v = C_d \frac{A_p A_t}{\sqrt{A_p^2 - A_t^2}} \sqrt{\frac{2g}{\alpha}(P_p - P_t)} \tag{2.6}$$

where C_d denotes the discharge coefficient (for standard venturi meters is between 0.96 to 0.99), A_P presents the area of approach piping (upstream), A_t is the area of throat section, g is the acceleration of gravity (9.81 m/s^2), α is velocity distribution coefficient (1.02), P_P is the upstream pressure (in unit Bar) and P_t is the throat pressure.

Therefore, the above equation can be used in this study to determine the system flow rate using pressure drop measurements ($P_P - P_t$) obtained from the venturi meter.

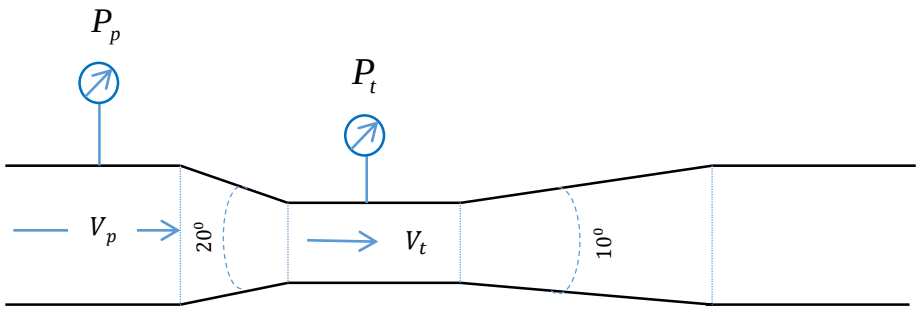

Figure 2.5. The schematic diagram of a venturi meter (ISO 5167)

2.4. Fault Simulation

Corrosion and external solid materials in fluids are major factors that can lead to impeller damages. Two main faults are simulated in this study, namely cracking and imbalance. Each defect consists of three severity levels of damage staged on the pump impeller (low, medium and high). A series of damages are simulated from small to the large in terms of damage size to test the effectiveness of the automated health monitoring method. The photograph in figure 2.6 depicts the type of closed impeller used on this study. As it is shown, the location of cracks are on the plate close to the impeller eye and the imbalances are located at the top plate close to the end of impeller vane.

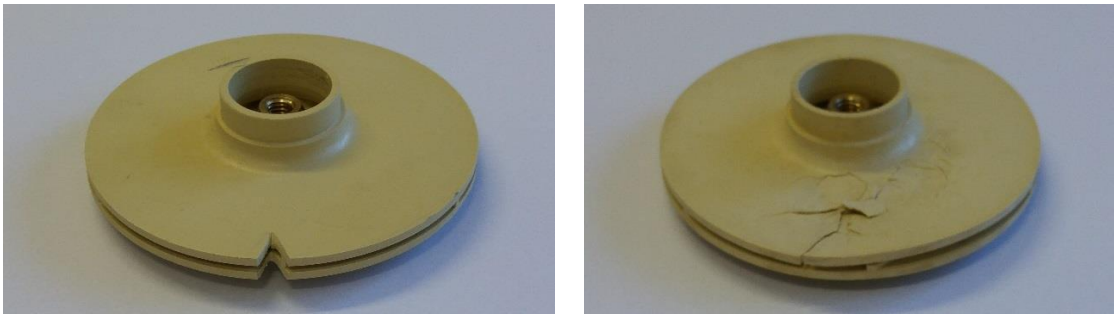

Figure 2.6. An illustration of common damages induced to an impeller (left) Unbalanced impeller, (right) Impeller with crack

As the size of damage increases, the severity of the damage increases as well. Impeller cracking was simulated on the plate close to the impeller eye by using a hammer blow. There are eight operational conditions in this study, namely the normal condition (N), cavitation and six faulty conditions with six different severity of damages.

In order to detect the different impeller faults as shown in figure above, six kinds of cracks and imbalances are induced as follows: (1) The lengths of crack are approximately 10 to 50 mm and located in the side of impeller. These damage states are denoted as Fault 1, Fault 2 and Fault 3, respectively. (2) The lengths of imbalances were 4, 8 and 12 mm, and located close to the gap between two plates. These damage states were denoted as Fault 4, Fault 5 and Fault 6, respectively. Table 2.2 outlines the fault types and the relevant dimensions staged on the pump impeller.

Table 2.2.Specifications of the impeller damages

Fault No.	Fault Type
Fault 1 ($C1$)	Crack size ≃ 10 mm
Fault 2 ($C2$)	Crack size ≃ 20 mm
Fault 3 ($C3$)	Crack size ≃ 30 mm
Fault 4 ($U1$)	Unbalance size ≃ 4 mm
Fault 5 ($U2$)	Unbalance size ≃ 8 mm
Fault 6 ($U3$)	Unbalance size ≃ 12 mm

Moreover, a clear PVC pipe is utilized in input and output of the experimental pump to visually observe cavitation phenomena in the system.

2.5. Summary

The main purpose of developing a pumping system in this study is to: (i) Simulate the various failure modes on a centrifugal pump impeller under varying conditions. (ii) To observe the performance of condition monitoring tools on the evaluation of vibration signals. (iii) Identifying the relation of different impeller damages for the purpose of intelligent fault diagnosis as shown in figure 2.7.

Furthermore, the structure of the experimental setup and the details of instruments are elaborated on and the following topics are contributed in this chapter:

- Required specifications of pumping system
- Numerical procedures on flow and pressure measurement
- Details on design of a venturi meter based on the measurement of pressure difference in the system according to the standard ISO 5167
- Simulation of the impeller common defects

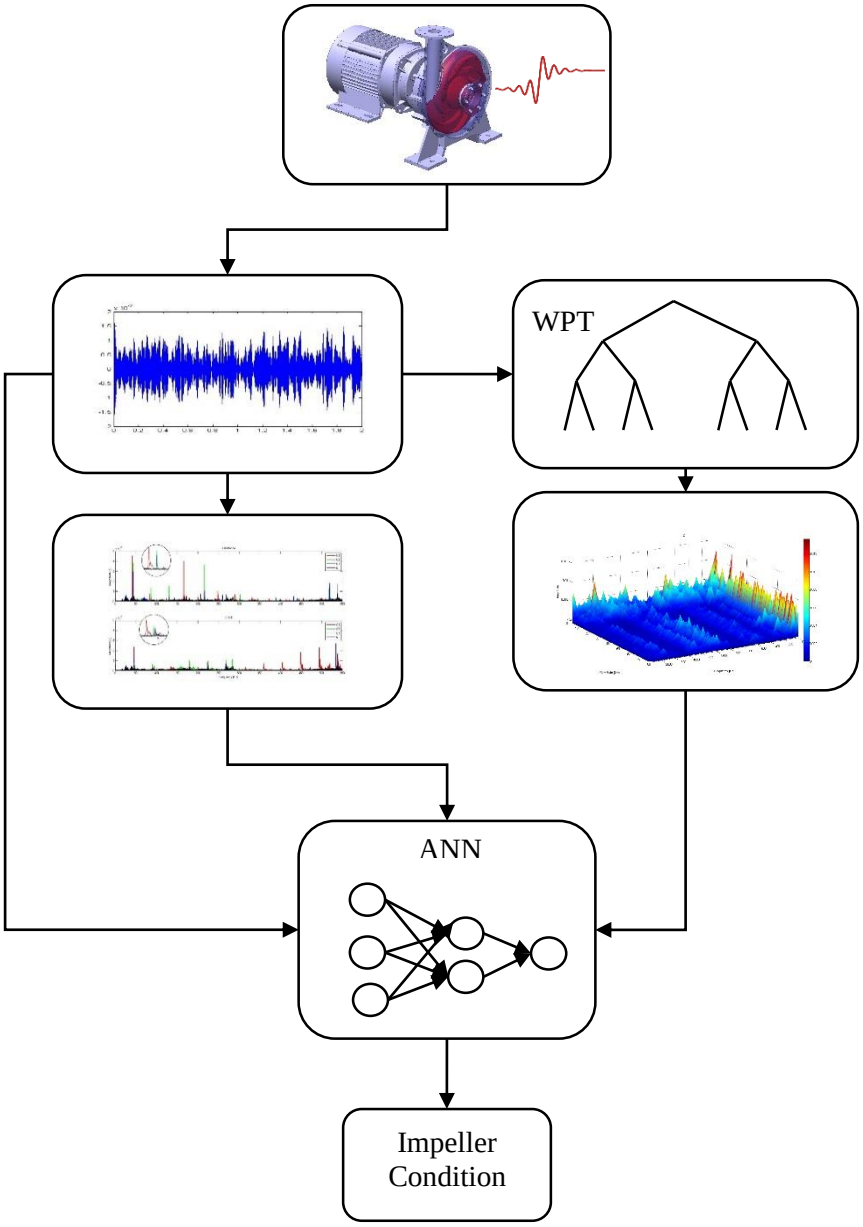

Figure 2.7. Intelligent fault diagnosis procedure

3. Signal Analysis (Data Analysis)

3.1. Introduction

This chapter presents the analysis of vibration signals generated by the experimental setup using types of faults with varying severities in impellers. Measurements are made to identify the fault type and characterise the system condition. In order to provide a visual presentation of the vibration signature, the collected data is examined using time, frequency and time-frequency analysis methods, respectively.

According to the effect of faults on the performance of centrifugal pumps, the significant vibration frequencies that contain useful information related to the impeller conditions are explored. These frequencies are the pump frequency (rpm), its harmonics (mostly second, third, and fourth harmonics) and the vane passing frequency (Taneja, 2013). This chapter also covers the evolution of signal characteristics over different flow rates. In addition, in the last section a comparison of all three analysis methods is provided.

3.2. Data Collection Procedure

The experimental data on this research work is collected as the illustrated procedure in the figure below:

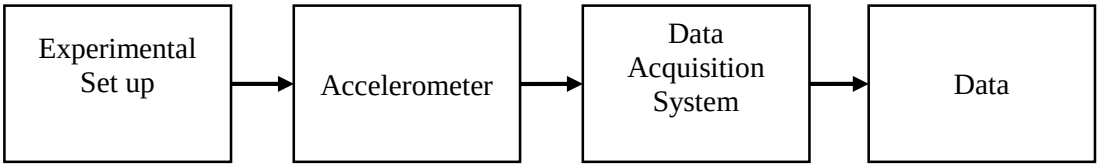

Figure 3.1. The experimental procedure

The experimental setup of the water centrifugal pump system is shown in figure 3.2. A two pole induction motor drives the pump and allows the pump to operate up to 2700 rpm. A control valve is used to control flow at the inlet of pump. In addition, an inlet valve is used to create pressure drop between the suction and at the eye of impeller to simulate flow fluctuation.

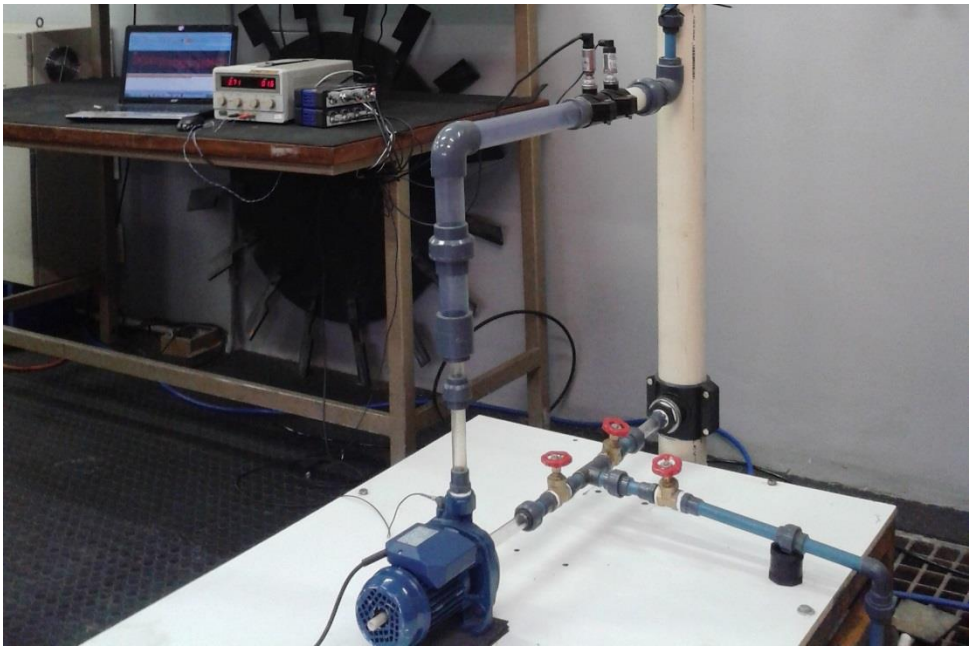

Figure 3.2. Experimental apparatus

Moreover, a triaxial accelerometer with sensitivity of 10 mV/g is used to collect the vibration signals, which is mounted on top of the impeller casing. A Quantum X - 4 channel data acquisition system is used to collect data from the accelerometer and pressure transducers, which is controlled by the Catman professional data acquisition software.

For the purpose of this study, the digital data is collected at 9600 samples per second to obtain the influence of defects and cavitation over a wide frequency range. It was later downsampled to 4800 samples per second which is a sufficient frequency range for the signals considered in this research.

Additionally, a tachometer is installed to detect the exact rotational speed due to the fact that impeller defects under consideration in the present study, have significant effects on the pump rotational speed. The tachometer is positioned along the end of rotor shaft of the electric motor that is extended by adding a nylon shaft. Figure 3.3 depicts the location of tachometer and accelerometer. The coordinate system used in this study is shown in figure 3.3.b, where X and Z directions denote the measured radial vibration, and Y denotes the axial vibration. Also the designed venturi meter is used to measure the flow rate of the system. Therefore, two pressure sensors were installed to measure water pressure simultaneously.

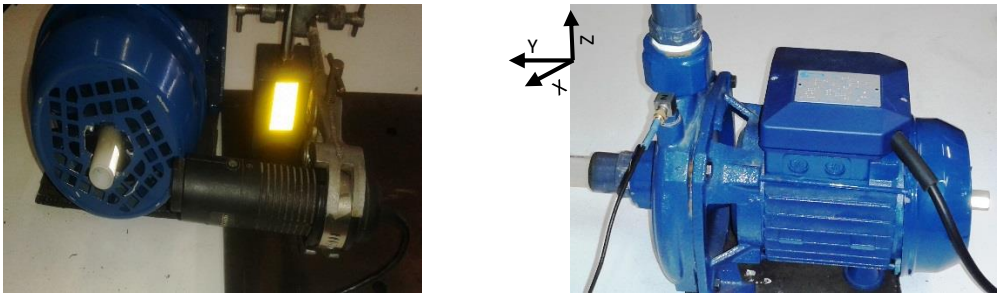

Figure 3.3. Location of (a) Tachometer, (b) Accelerometer

In order to collect the signals regarding the induced conditions, faulty impellers were installed in the test setup and vibration data was acquired using the accelerometer. The experiment was run under two circumstances. Firstly, data samples were collected at a constant flow rate of 60 l/min. A time signal of 576000 of data samples was collected in each experimental run, and the rotational speed of the motor was in range of 2700 to 2800 rpm. Secondly the data points were collected under flow variation in between 0 to 90 l/min in order to investigate on flow fluctuation to demonstrate the repeatability and to obtain statistically significant results. A total number of 4 measurements for each simulated condition each containing a data set of 259200 samples, are conducted over 27 seconds. Among seven impeller damage conditions, there are 12 vibration signals for each condition, hence 84 raw vibration signals are measured in total.

3.3. Data Analysis

In the present section, the results obtained from the time domain analysis (TDA) will first be discussed. The section then discusses the results obtained from frequency analysis (FA) and finally the results from time-frequency analysis (TFA) are evaluated. The last section presents the parameter extraction to determine the seven impeller scenarios. All three methodologies are complemented by comparison of extracted features for an over view of fault indicators in each signal.

3.3.1. Time Domain Analysis

As noted in chapter one (section 1.3.4.1), TDA computes statistical parameters from the vibration data and applies a comparison process in order to identify signs of faults. In this section an evaluation process on overall vibration measurement is being provided. This

evaluation depicts the evolution of statistical parameters over the period of measurement, and also describes the amount of vibration energy being created by impeller.

Vibration signal data has been measured over 60 and 27 seconds under two conditions: (a) a constant flow rate of 60 l/min and (b) flow variation, respectively. Eight statistical features are extracted from each signal to form a pattern with regard to the impeller condition. According to the approach discussed in the literature study (section 1.3.4.1) mean μ, root mean square RMS, kurtosis K_t, skewness S_n, energy E, crest factor C_r, standard deviation S_t and impulse factor IF are the eight statistical parameters used for TDA in this section. These features are therefore normalized by dividing data sets with the corresponding maximum values.

Thereby, for seven conditions of impeller, figure 3.4 shows the normalized features for a constant flow rate of 60 l/min over a period 60 seconds. Each plot represents a specific feature in the measured axis (vertical, horizontal and axial). It should be noted that referring to the table 2.2 (chapter two), the parameters $N, C1, C2, C3, U1, U2$ and $U3$ denote the seven conditions of impeller as follow: normal impeller N with no prior defect, impeller $C1$ with the crack size of 10 mm, impeller $C2$ with the crack size of 20 mm, impeller $C3$ with the crack size of 30 mm, impeller $U1$ with the imbalance size of 4 mm, impeller $U2$ with the imbalance size of 8 mm and the impeller $U3$ with the imbalance size of 12 mm.

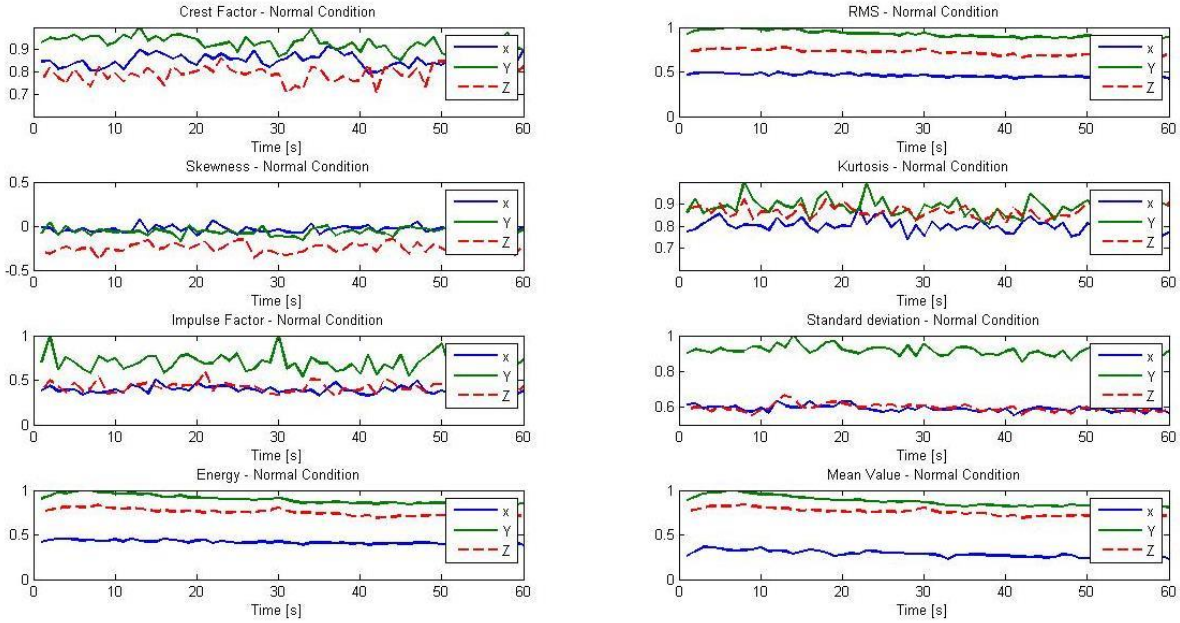

Figure 3.4. Time domain features over 60 seconds for a constant flow rate

Figures 3.5 and 3.6 show the time domain features (TDF) over flow variation for both normal and crack level one.

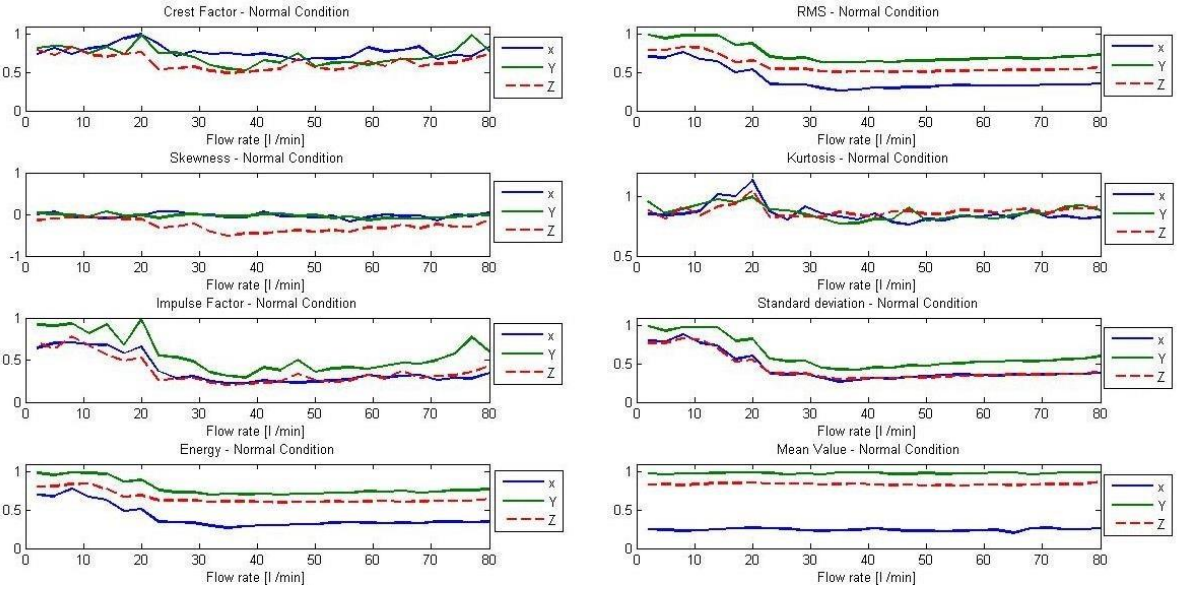

Figure 3.5. Evolution of TDF under variable flowrate for a normal impeller

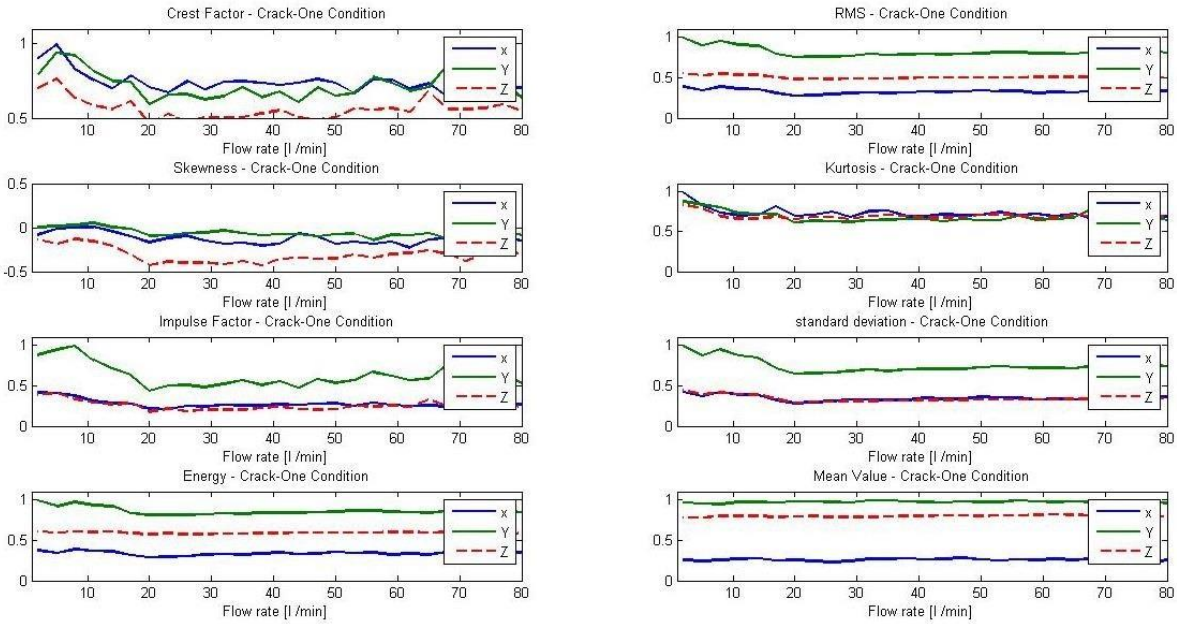

Figure 3.6. Evolution of TDF under variable flowrate for a damaged impeller – C1

A careful consideration of the figures above indicates apparent difference in vibration level for axial direction (Y axis) except in kurtosis, skewness and crest factor. It is due to the applied defects on the impellers which led to asymmetric flow in the system and caused

larger flow impacts and higher level of vibration in axial direction. Figures below illustrate features of all conditions against each other over flow variation.

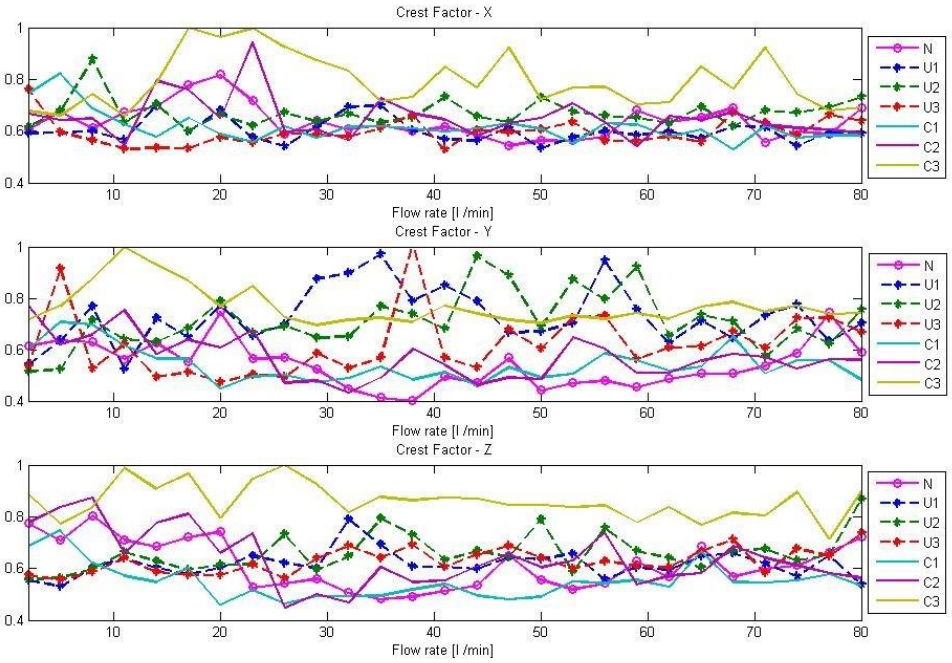

Figure 3.7. Crest factor evolution under variable flowrate

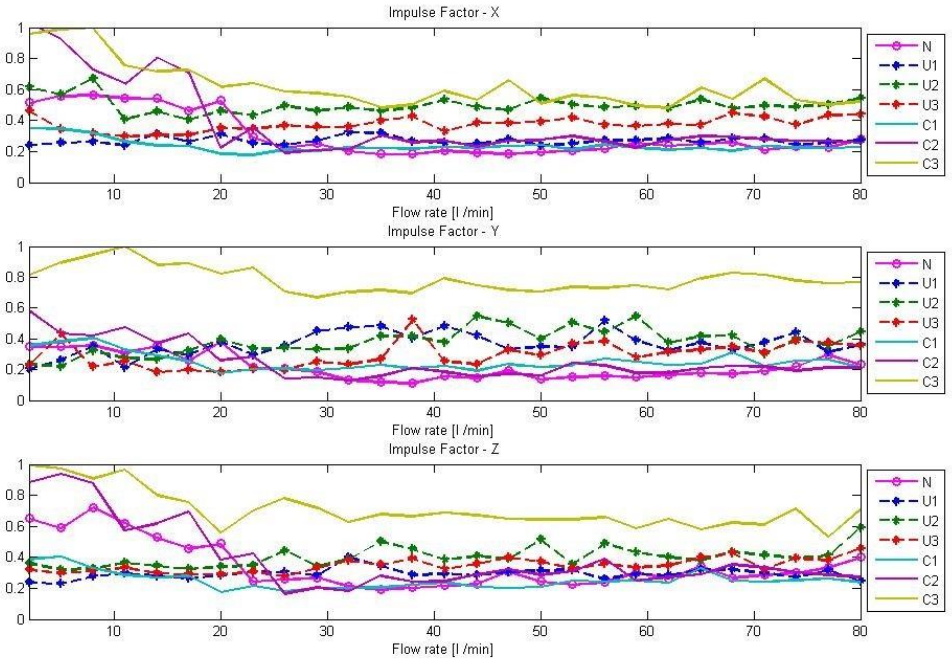

Figure 3.8. Impulse factor evolution under variable flowrate

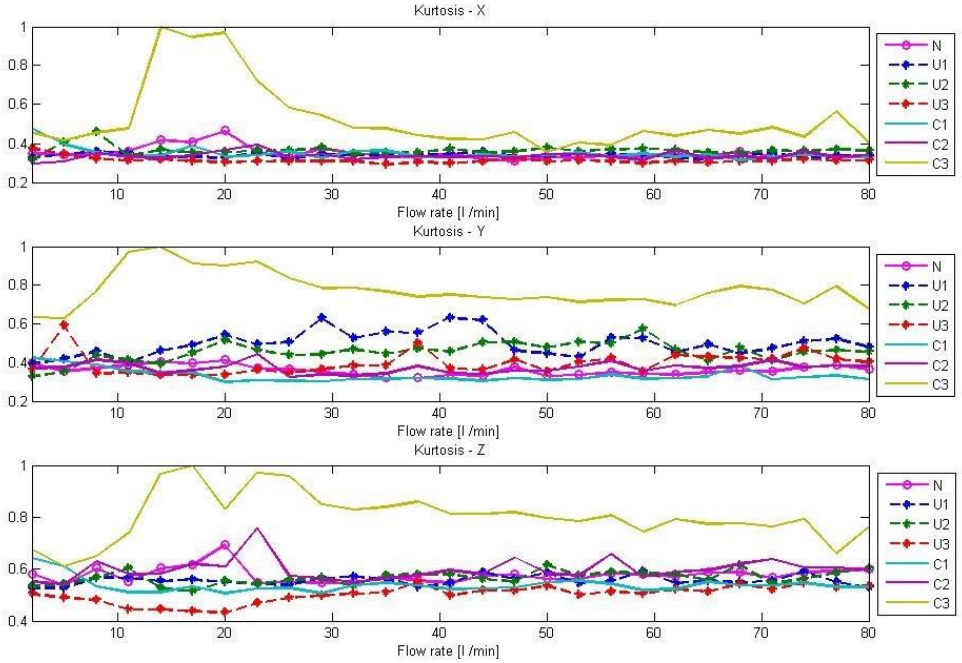

Figure 3.9. Kurtosis evolution under variable flowrate

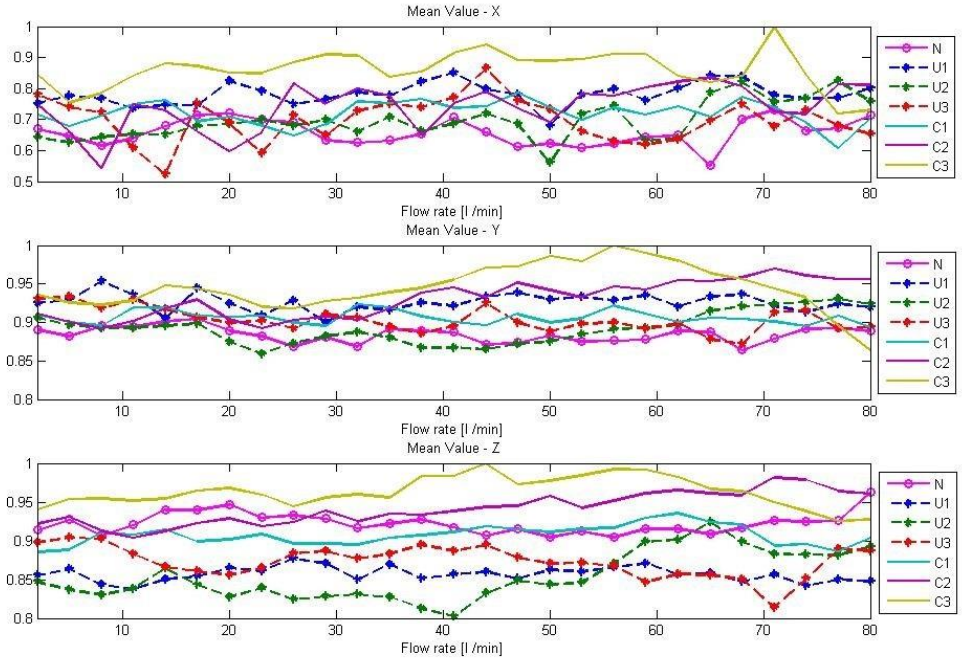

Figure 3.10. Mean value evolution under variable flowrate

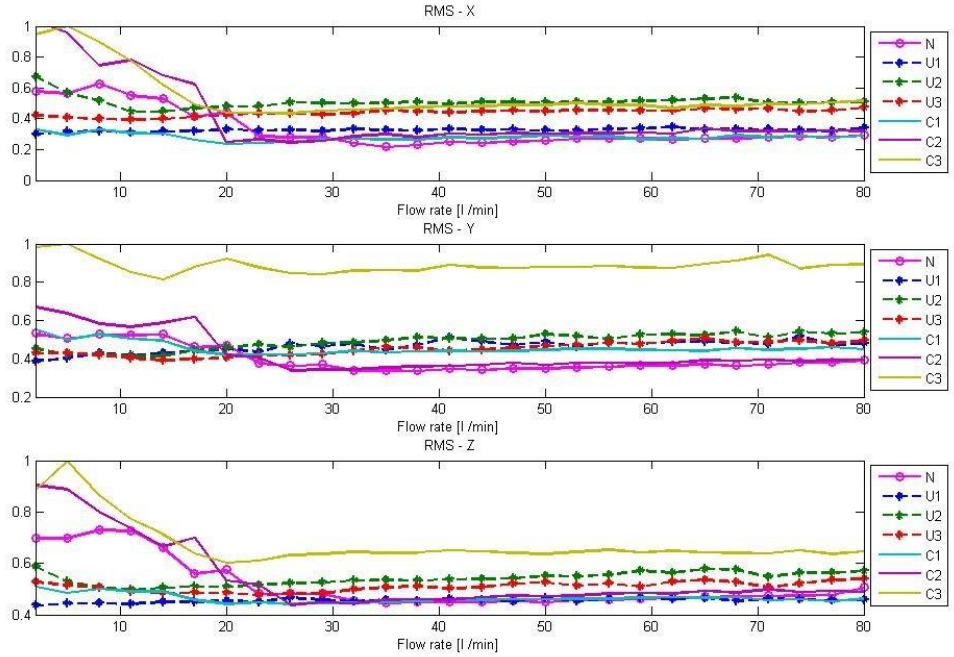

Figure 3.11. RMS value evolution under variable flowrate

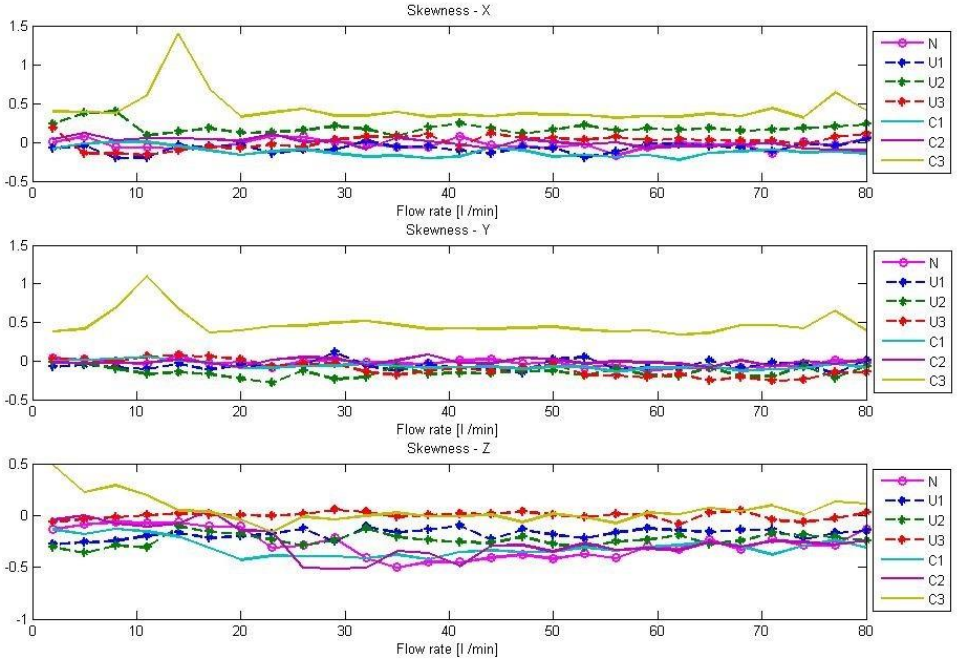

Figure 3.12. Skewness evolution under variable flowrate

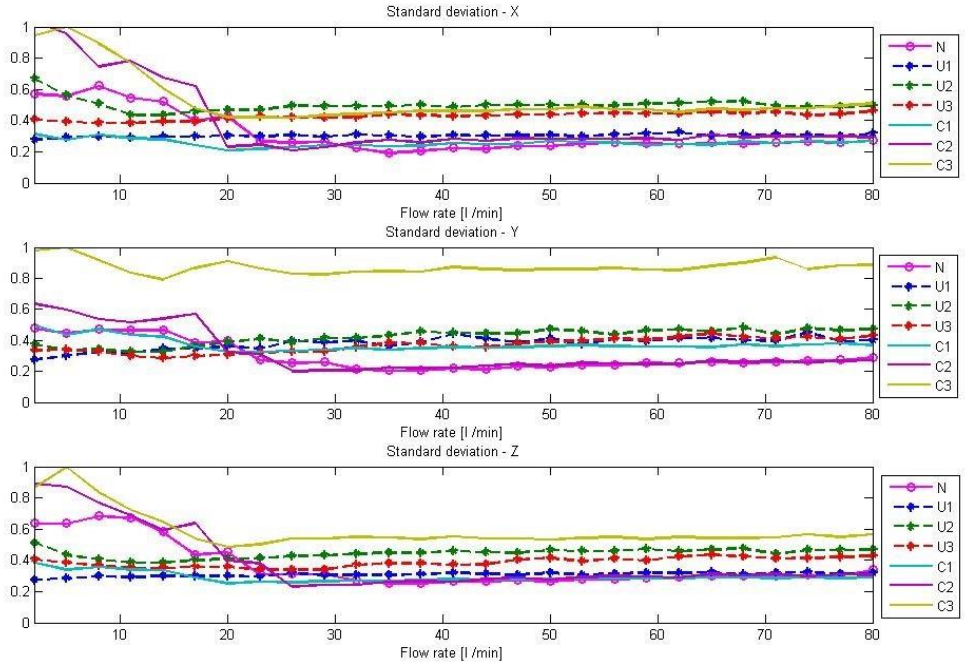

Figure 3.13. Standard deviation evolution under variable flowrate

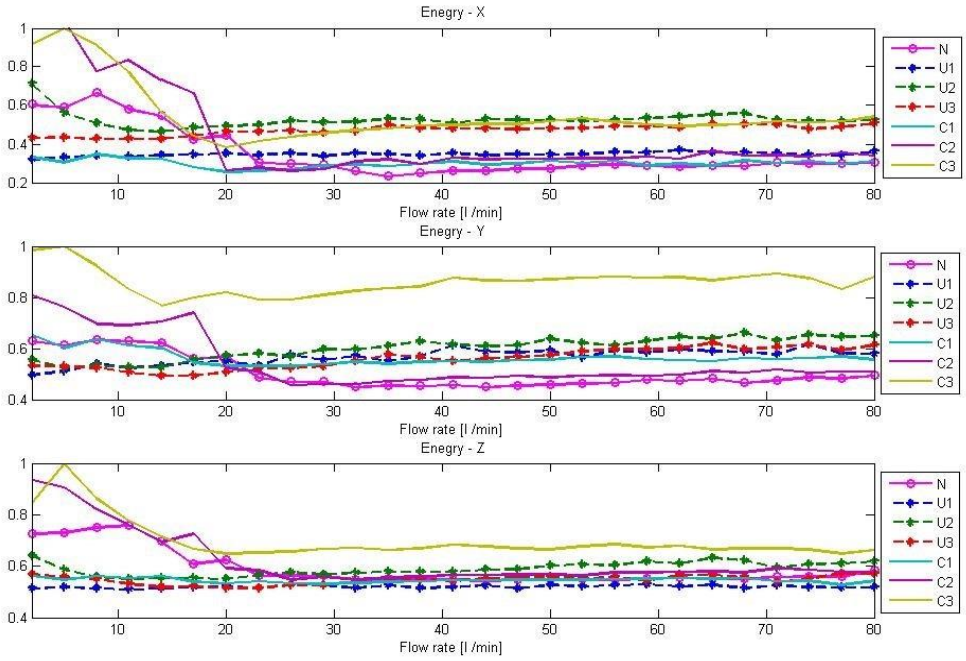

Figure 3.14. Standard deviation evolution under variable flowrate

From the figures 3.7 to 3.14, it can be stated that signals from axial direction provide more reliable information regarding to the operating condition. It is also clear that the vibration

characteristics have higher magnitude for the flow rates lower than 20 l/min which is due to the cavitation in the system. On the other hand, some features such as crest factor and mean value do not exhibit an explicit pattern. Also it can be seen that the crack has higher impact on the vibration magnitude, while C3 has higher energy value compare to imbalance. This is due to the fact that cracks have made changes in impeller geometry and resulted in a significant change of flow path. Thereby, RMS and standard deviation features display more reliable features than others.

Thus, it can be deduced that some features do not contain detectable information, since the analysis is being performed for more measurements and ambiguous patterns were observed. Hence, it is very important to choose the right features with the lowest uncertainties.

3.3.2. Spectrum Analysis

As mentioned in section 1.3.4.2, the pump frequency and the corresponding harmonics and the vane pass frequency are to be considered as valuable and indicative parameters. Also it is mentioned that the influence of cavitation, which may occur at the impeller eye, emerge as higher level of energy in high frequencies.

Vibration signals are therefore analysed in frequency domain to identify efficient features for the seven data sets collected from the impeller under various conditions. Spectrum analysis helps to achieve a better understanding on impeller vibration responses. It also displays a more detailed view of significant components on frequency domain such as rotational speed frequency, related harmonics and vane passing frequency. Figure 3.15 shows the frequency spectra of a normal impeller in axial and radial directions.

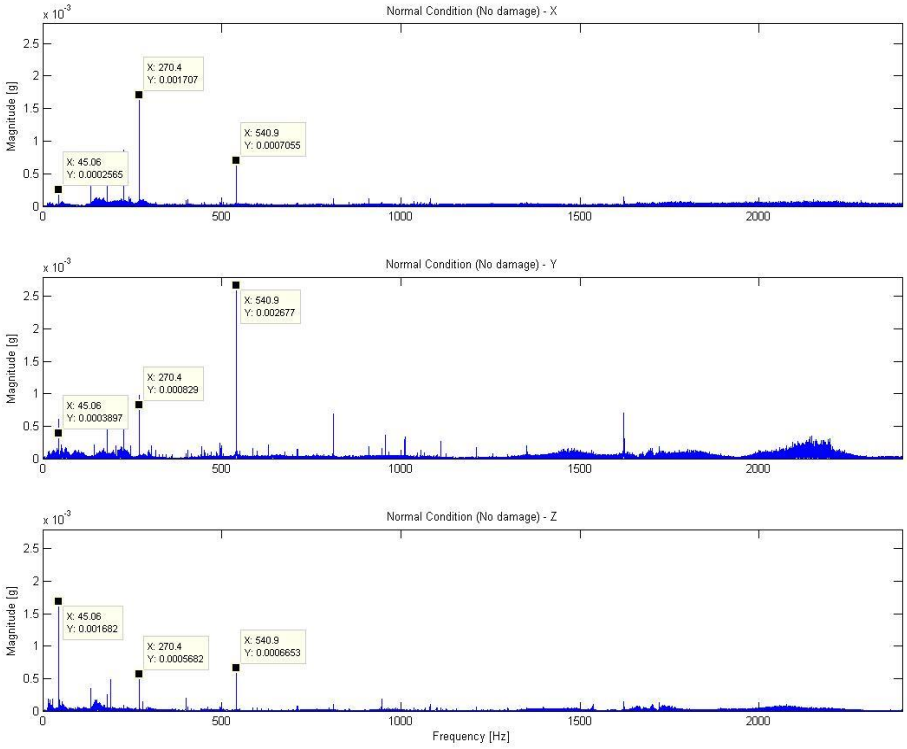

Figure 3.15. Frequency spectra of an impeller with normal condition in axial and radial directions

Figure 3.15 presents the vibration response for the impeller with no prior damage at a constant flow rate. A comparison of amplitude in all directions, indicates that the frequency components on axis Y show higher levels of energy. This can be due to the fluctuating pressure from the interaction of flow and impeller, flow turbulences, cavitation and hydraulic pulsation. As marked in the figures above, the pump rotational speed (rpm), the sixth harmonic of the pump rotational speed (6×rpm) which corresponds to the impeller vane pass frequency (VPF) and the second harmonic of the VPF (2×VPF) can easily be identified with high amplitudes.

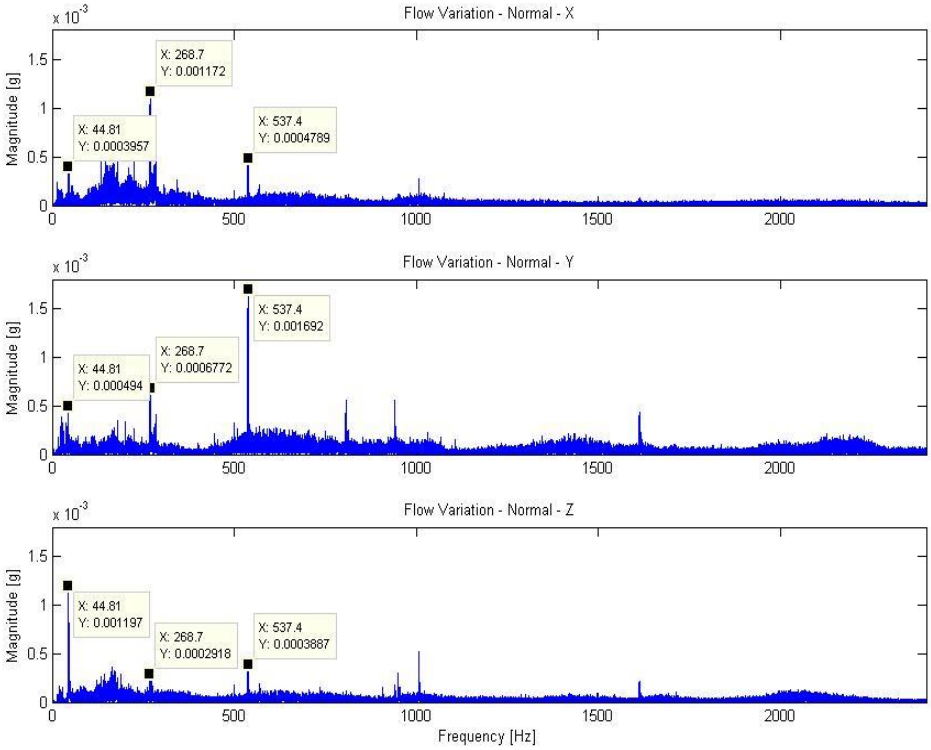

Figure 3.16. Frequency spectra of the three vibration signals

Figure 3.16 shows an impeller with normal condition over varying flow rate. The flow variation helped to simulate zero flow rate, low flow rate (cavitation) and flow at pump BEP (best efficiency point), which is expected the system to have the highest performance at BEP.

An examination of figure 3.15 and figure 3.16 indicates a significant increase of noise level in Y and Z directions under the flow fluctuation. However the direction X shows almost a constant level of noise. Moreover, the frequency components (1 ×rpm, VPF and 2×VPF) in figure 3.15 have lower amplitude.

Figure 3.17 presents frequency spectra of two induced damages with the relevant severity over varying flow rates in radial direction. It can be stated that crack *C* influences the higher harmonics of rpm. However, unbalanced condition *U* affects the first rpm and VPF.

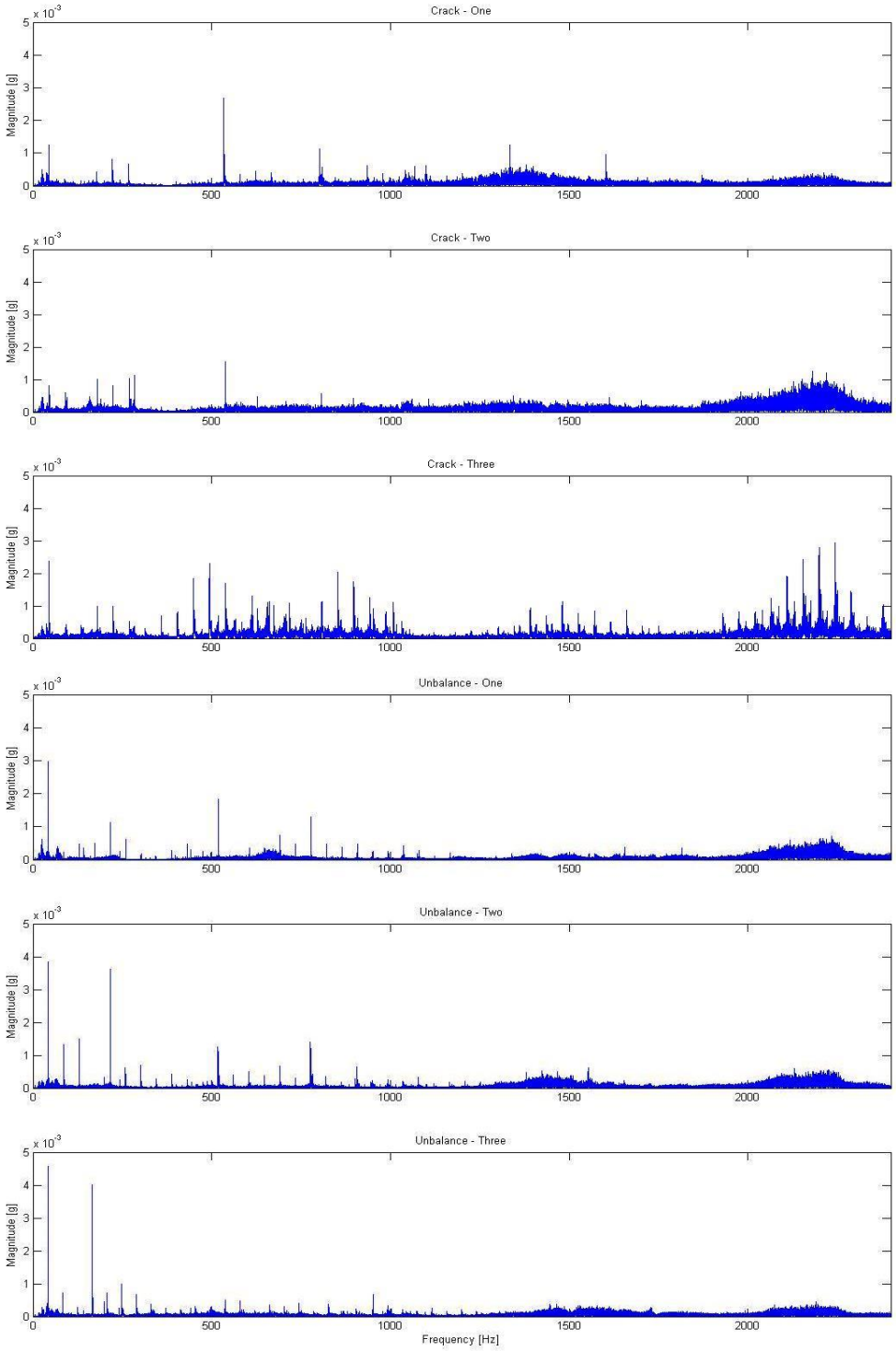

Figure 3.17. Frequency spectra of the induced defects

(Top to bottom: C1, C2, C3, U1, U2 and U3)

As described in chapter one, vibration characteristics are propagated over a wide range of frequencies. Hence in this section, signals are studied over two frequency ranges, low (1 Hz to 1kHz) and high (1kHz to 2.4kHz) frequency ranges, respectively. Furthermore, as it was discussed in the literature (section 1.3.4.2) a higher vibration amplitude can be observed for the measured data in axial direction. Thus, the vibration data of axial direction is chosen for the further analysis due to its high sensitivity to the impeller condition.

a) Spectrum Characteristics of Low Frequency Range:

Figure 3.18 captures the spectra of three vibration signals corresponding to impeller conditions, namely no damage (N), crack (C1, C2, C3) and unbalanced impeller (U1, U2, U3) with the correlated severities (table 2.2-chapter 2) in frequency domains. The low frequency range plot depicts nearly the same broad band which is influenced by the flow turbulence. Also fundamental frequency components are visible with higher amplitude. These components are due to the interaction between flow and impeller vanes.

Figures 3.18 (a) and (b) present a comparison between unbalanced condition and crack with increasing damage severity (U1 to U3 and C1 to C3) against the impeller with normal condition. It indicates that the 1×rpm amplitude increases as severity of the damage increases. However, imbalance effects appear in higher amplitude than crack, while the second to fifth harmonics of the rpm frequencies are excited. On the other hand, crack excitation appear more visible in the 8^{th} to 11^{th} harmonics with higher amplitudes.

In addition, both figures display a significant difference in frequency location for each damage severity. The pump speed and the severity of damage appear to be inversely proportional, which the pump rotational speed for a normal condition is appeared at 45 Hz (2700 rpm), while the rpm for U3 condition is presented in 41.33 Hz (2480 rpm).

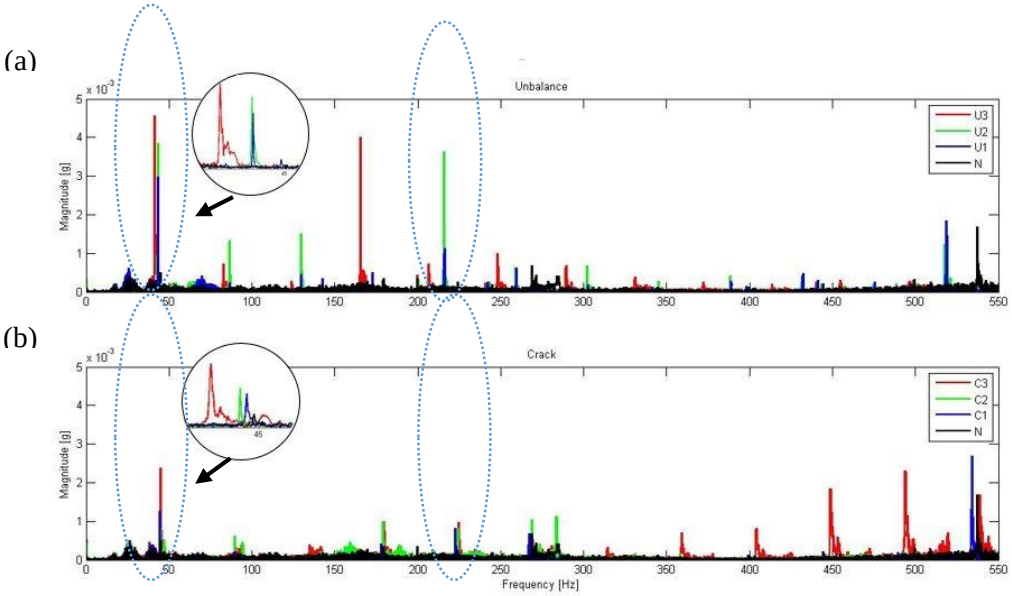

Figure 3.18. Vibration spectra of low frequency range, (a) Unbalanced impeller vs normal (b) Impeller with crack vs normal

b) Spectrum Characteristics of High Frequency Range:

Figure 3.19 presents the frequency spectra of the introduced conditions (table 2.2). Comparing the spectral differences between N, C and U with corresponding severities, it can be identified that the broadband in damaged conditions has higher amplitude. In addition, the high orders of rpm are excited more in crack conditions than in imbalance. Also spectral energy is increased significantly in frequencies over 2000 Hz, where it can be due to the pressure drop in the suction of the pump while the flow rate was restricted by closing the suction valve. Moreover, as U3 has higher amplitude in comparison to U2, U1 and N in figure 3.19 (b), it indicates increasing vibration energy in the harmonics of rpm by increasing the severity of defects.

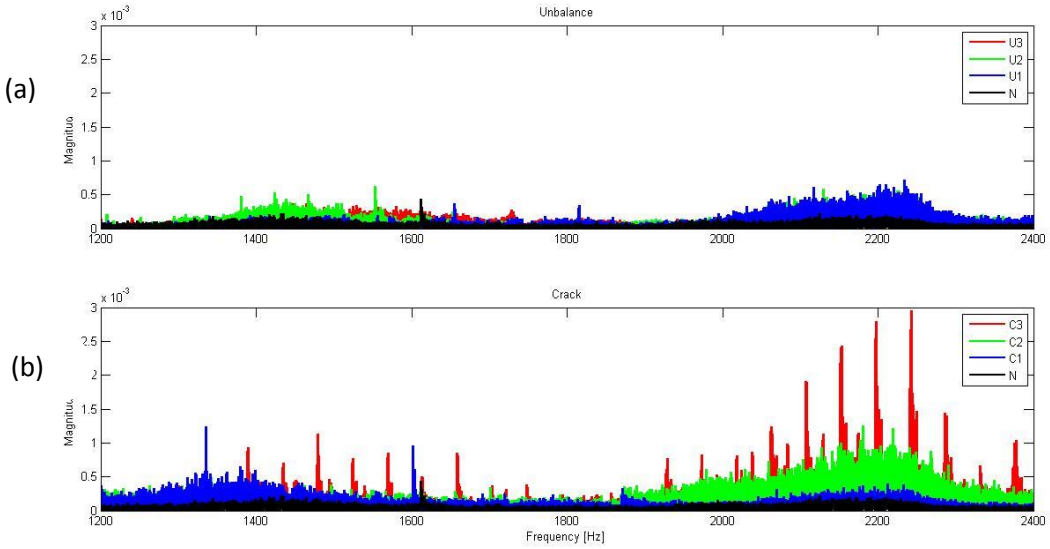

Figure 3.19. Vibration spectra of high frequency range, (a) Unbalanced impeller vs normal (b) Impeller with crack vs normal

As shown in previous figures, it can be seen that the amplitudes of the normal impeller at the shaft rotational frequency, its harmonics and broad band energies in higher frequency ranges are different from the impellers with faulty condition. Considering the fact that the amplitudes and energy bands may contain prominent information associated to the degree of defects or the conditions of impeller; and since the system is considered to be run under fluctuating flow conditions, it is adequate to study the fundamental frequency amplitudes and broadband energies over variation of flow.

Figure 3.20 illustrates the evolution of five frequency components against the varying flow rates (zero to 80 l/min) and the impeller conditions. The pump frequency, its sixth, 12^{th} (2×VPF), 18^{th}, and 36^{th} harmonics are extracted as valuable information in axial direction, and all the other higher frequencies are considered as broadband frequencies.

As mentioned before, running under required flow rate of a pump, will influence the frequency amplitudes. Figure 3.20 (a) shows the 1×rpm amplitude against flow rate, indicating higher imbalance amplitudes in compare of cracks. It is also apparent in figure 3.20 (b) that imbalance effects are remarkable, which the lower flow rates caused amplitude drops. However, it does not show any specific behaviour between defects and flow rate.

It can be deduced from Figures 3.20 (c), (d) and (e) that the influence of crack damages become more explicit as the number of harmonic orders increases. In addition, the

frequency component at pump vane passing frequency and high orders of harmonics indicate lower amplitude for unbalance condition, which may be due to the less contact between vanes and flow.

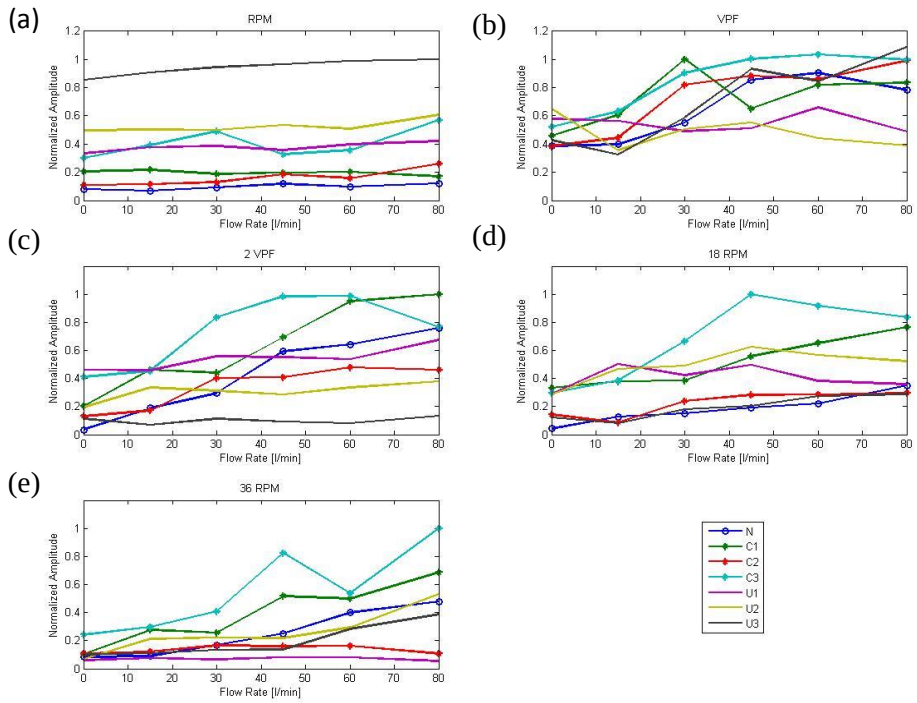

Figure 3.20. Amplitude evolution of frequency components against flow rate, (a) 1×rpm, (b) VPF, (c) 2×VPF, (d) 18× rpm, (e) 36×rpm

3.3.3. Time-Frequency Analysis

In this section, the objective is to decompose a time series into time-frequency space. Therefore, the same vibration data used in TA and FA is being used. Initial data is collected in sampling rate of 9600 Hz. In order to increase frequency resolution and be able to observe fault effects, the measured signals are resampled in sampling frequency of 4800 Hz. Afterwards, wavelet packet transform (WPT) mentioned in chapter one section 1.3.4.3, is applied on the measured signals.

WPT requires prior information such as level of decomposition and the appropriate type of mother wavelet, which determines the accuracy of the decomposed data. Considering the fact that there is no universal wavelet to perform for all types of signals (Phinyomark et al., 2009), hence the Daubechies wavelets such as db2 to db35 which are more preferable for WPT (Wang et al., 2015) are used to apply on the signals in this section.

For the purpose of this study, the db20 wavelet shows a better convergence with the generated signals. This wavelet has a better expansion performance and eases the handling of border issues. It also enhances the concentration degree of energy (Liao et al., 2009). Scaling function and wavelet function of db20 wavelet are shown in figure 3.21.

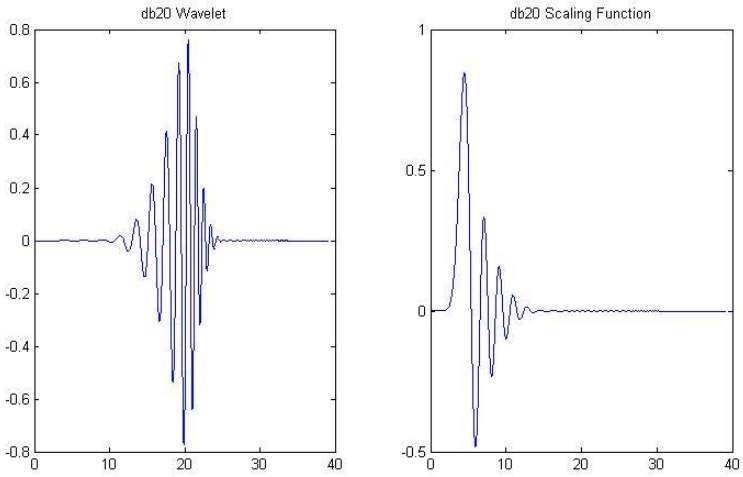

Figure 3.21. Scaling function and wavelet function of db 20 (Plotted using Matlab R2015a)

Wavelet based coefficients are created into different frequency subbands by applying WPT to the generated signals with regard to the level of decomposition. Vibration signals are decomposed up to 5 levels in order to obtain 32 frequency subbands in the present work. In order to increase the frequency resolution, each frequency subband covers only 75 Hz of frequency length. The corresponding frequency intervals are shown as in table 3.1.

Table 3.1. The frequency bandwidth of subbands

Subband	Frequency range (Hz)	Subband	Frequency range (Hz)	Subband	Frequency range (Hz)	Subband	Frequency range (Hz)
S1	0-75	S2	75-150 Hz	S3	150-225	S4	225-300
S5	300-375	S6	375-450	S7	450-525	S8	525-600
S9	600-675	S10	675-750	S11	750-825	S12	825-900
S13	900-975	S14	975-1050	S15	1050-1125	S16	1125-1200
S17	1200-1275	S18	1275-1350	S19	1350-1425	S20	1425-1500
S21	1500-1575	S22	1575-1650	S23	1650-1725	S24	1725-1800
S25	1800-1875	S26	1875-1950	S27	1950-2025	S28	2025-2100
S29	2100-2175	S30	2175-2250	S31	2250-2325	S32	2325-2400

The reconstructed signals acquired from the WPT decomposition, correspond to various frequency intervals. Figure 3.22 illustrates the decomposition process of a signal with WPT in this study. It represents WPT as a tree of low and high pass filters with five levels of decomposition. Each level consists of discrete frequency intervals (equal to 2^N). The original signal with sampling frequency of 4800 Hz is decomposed to low and high frequency components, namely approximations and details. In figure below f_N denotes the frequency band ($f_N = \frac{f_s}{2} = 2400Hz$). Also $X_{5,0}(n)$ to $X_{5,31}(n)$ are the reconstructed signals in level 5 with frequency length of 75 Hz.

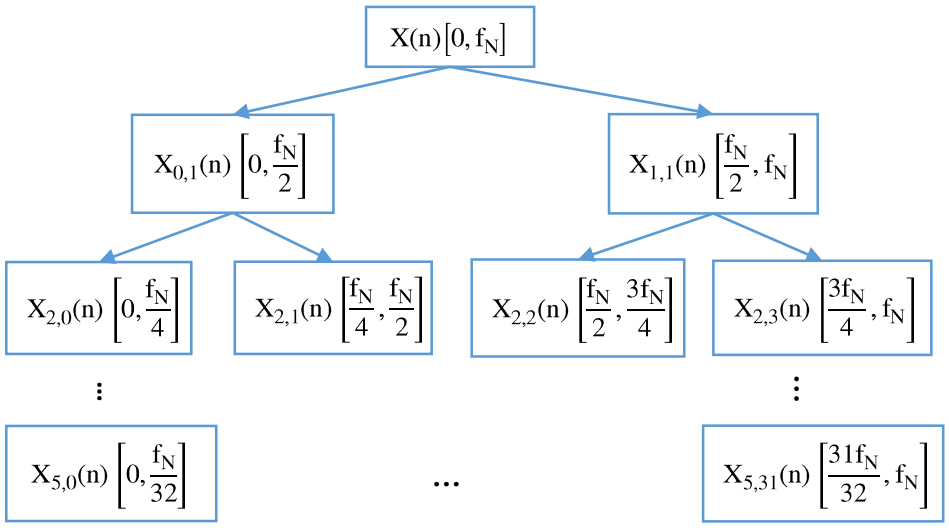

Figure 3.22. Wavelet package tree

Afterwards, signals are reconstructed from the wavelet coefficients relevant to each frequency band, and taken to the frequency domain. Figure 3.23 presents signal waveforms of all frequency bands after reconstruction for an impeller with normal condition. Moreover, a comparison between wavelet db10 and db20 is provided by figures 3.24 and 3.25.

From figure 3.25 it can be stated that the frequency bandwidths of the subbands obtained by the db10 implies the occurrence of frequency overlapping between different components. However, from figure 3.24 it can be found that the frequency ranges of the 1^{th} to 30^{th} components are about the mentioned frequency ranges, which satisfy the significant bandwidths. Therefore due to the observations, the db20 wavelet appears to be more reliable and can be used to transform the signals in to 5 level frequency bands.

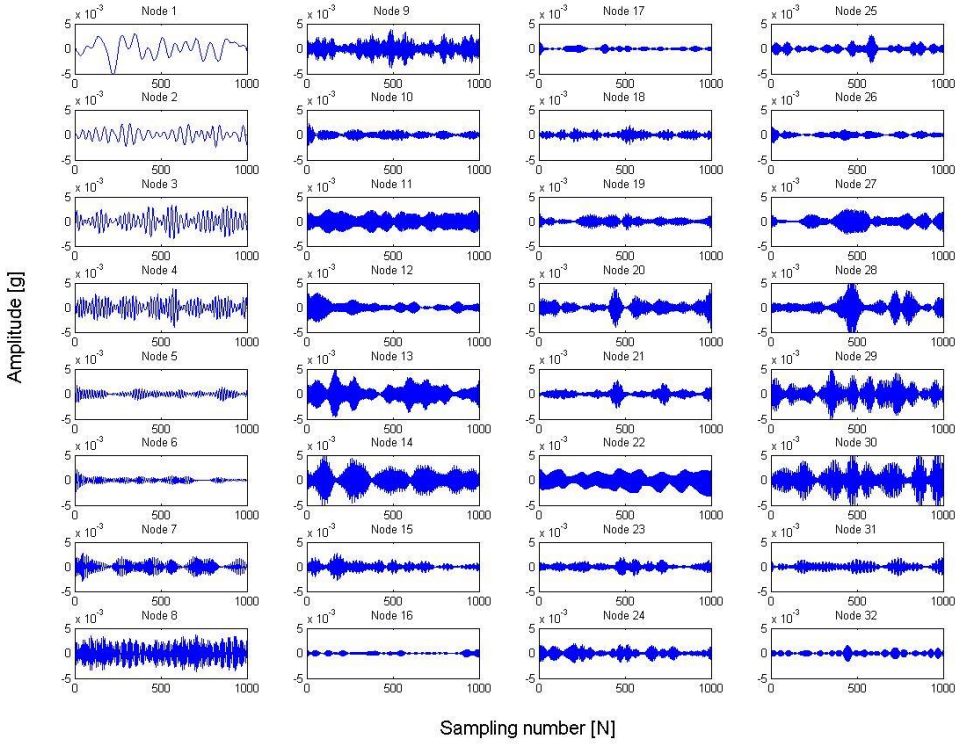

Figure 3.23. Reconstructed signals using db20 wavelet in level five - condition N

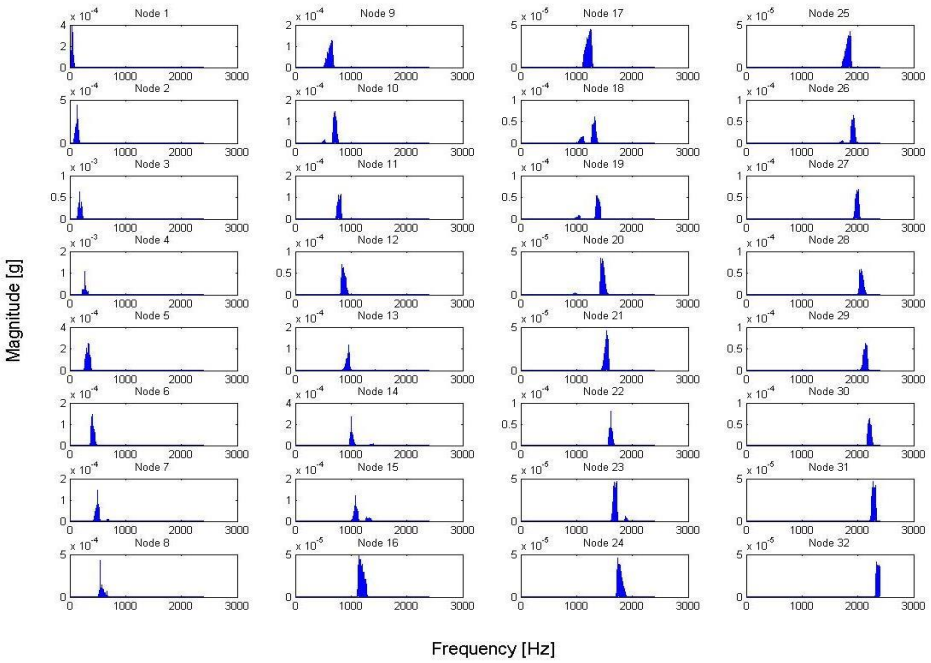

Figure 3.24. Fourier transform of reconstructed signals using db20 wavelet in level five - condition N

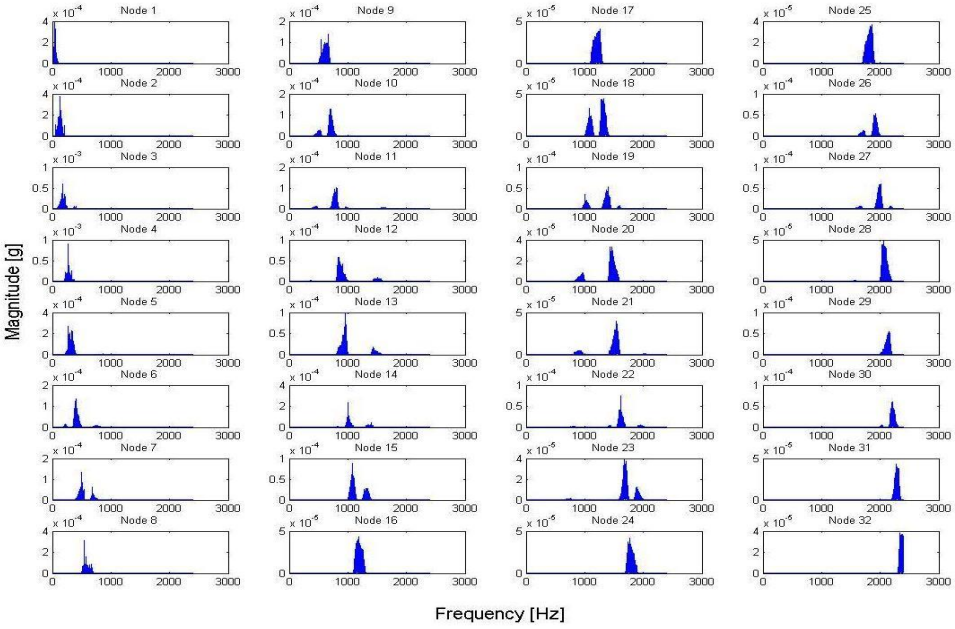

Figure 3.25. Fourier transform of reconstructed signals using db10 wavelet in level five - condition N

Figure 3.26 presents feature maps of impeller vibration in frequency and time simultaneously. It can be seen that flow rate affected the vibration energy, where the fundamental frequency components 1×rpm and BPF are clear in frequency range of below 300 Hz. The rpm and VPF frequencies, and other harmonics (like 18th rpm harmonic) are excited and significantly increased in low flow rates. In addition, in flow rates higher than 20 l/min, the minimum noise energy can be seen which only the 1×rpm and 5×rpm (VPF) are excited.

Crack and unbalance conditions with corresponding severities are presented in left and right columns of figure 3.27. The influences of cracks are appeared more in higher rpm harmonics, however unbalance effects are shown more in 1×rpm energy. Also, the background noise is increased in both defects for low flow ranges. However, despite of the normal condition, the noise energy is not seen to be minimum in faulty condition for flow rates over 20 l/min anymore.

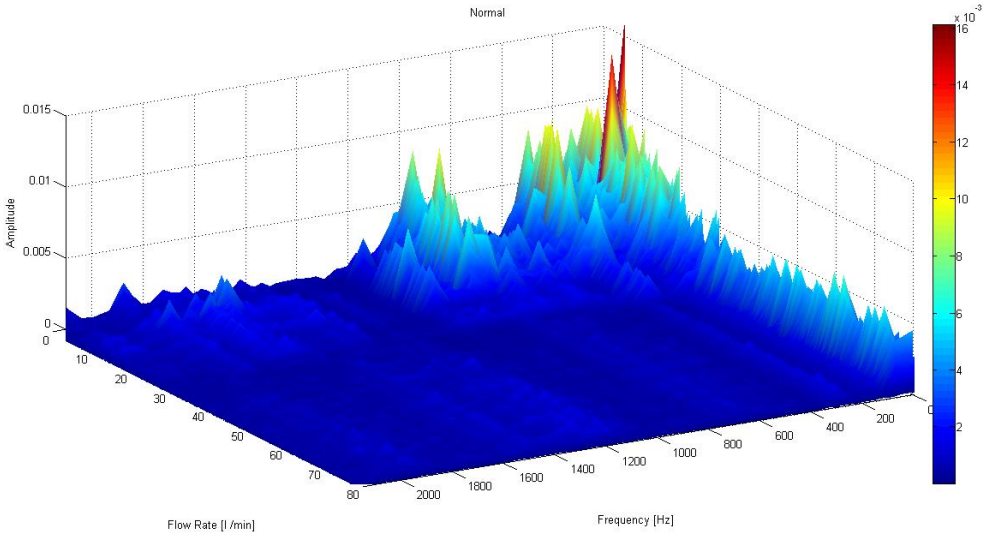

Figure 3.26. Time-frequency plot of an impeller with normal condition

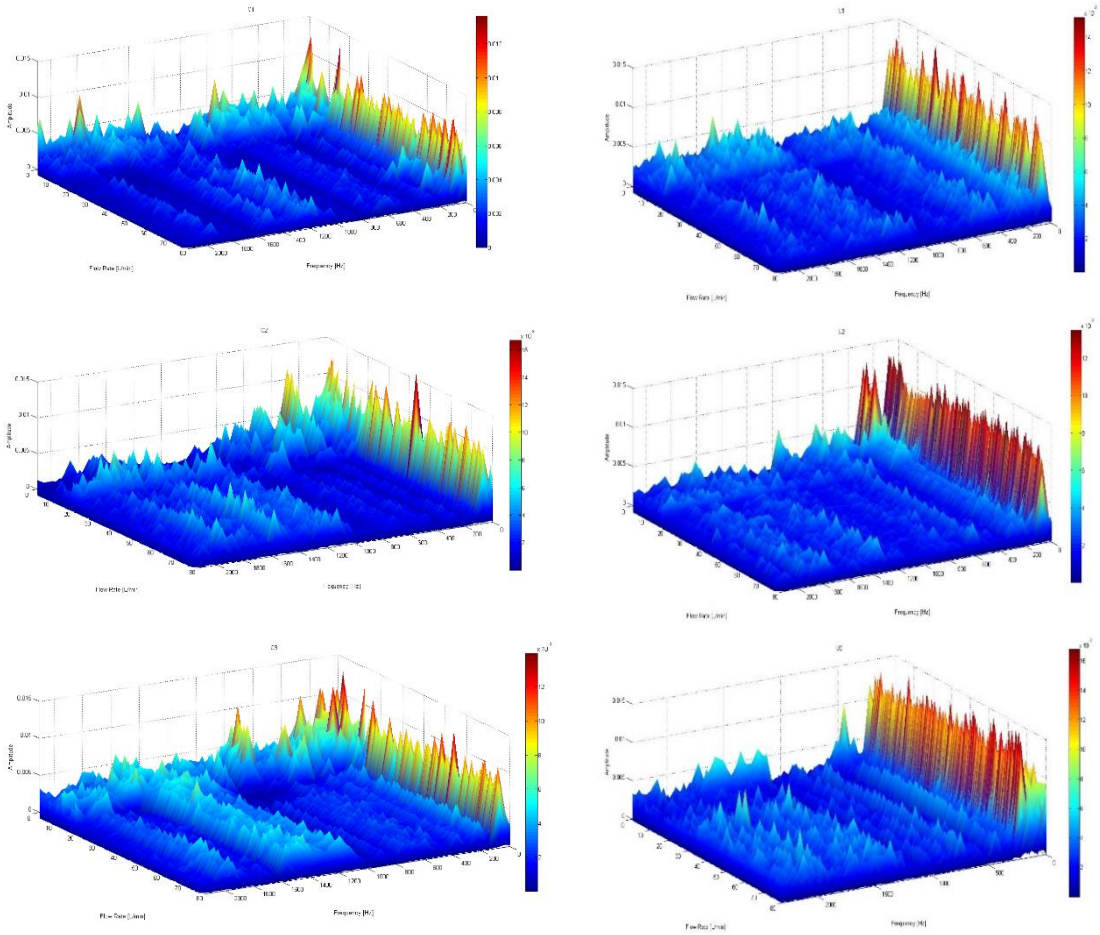

Figure 3.27. Time-frequency plot for impellers with faulty conditions: crack (left column), unbalanced impeller (right column)

As introduced in literature (section 1.3.4.3), the energy entropy is known as a good indicator to the behaviour of non-stationary vibrations in frequency subbands. Therefore, the energy entropy (equation 1.22) of various nodes of the decomposed signals are extracted to be used in determining the impeller condition.

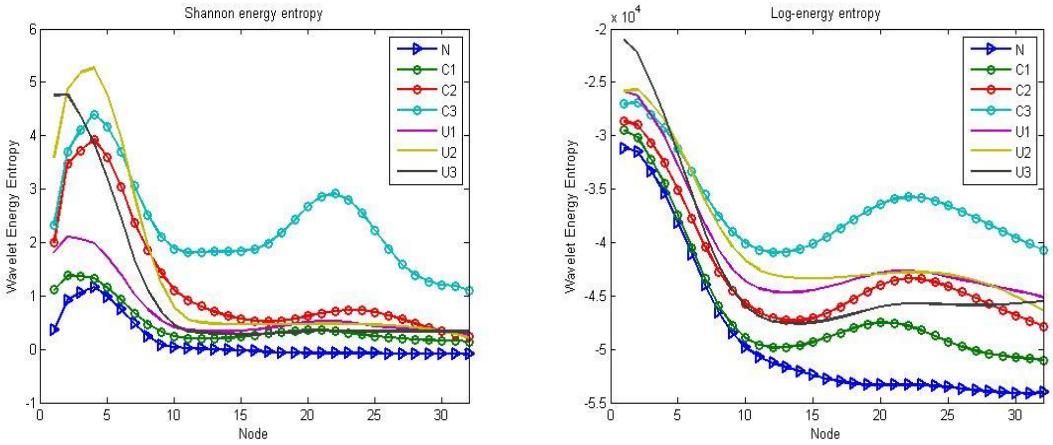

Figure 3.28. Comparison of two wavelet energy entropy of the signals in: Wavelet packet Shannon energy entropy (left); Wavelet packet log-energy entropy (Right)

Figure 3.28 depicts sample results of log-energy and Shannon energy distribution of frequency subbands 1 to 32 for vibration signals of normal and damaged impeller. From the figure it can be stated that the amount of energy held in the higher frequencies is high if crack is the impeller damage, while imbalance effects appear more in lower frequencies. Also log-energy represents the energy distribution of data more explicit than Shannon energy entropy.

Moreover, it can be seen that both energy distributions have interactions specifically in high frequency bands. However, log energy distribution emerge a more convenient information than Shannon distribution, and the lowest frequency bands are difficult to distinguish the fault severities. It must be noted that the data are being smoothed in Matlab software in order to be able to capture efficient patterns in each condition and reduce the influence of noisy data.

3.4. Summary

Fault detection as a critical step in condition monitoring requires a highly accurate method. In this section, three methods were studied, namely time domain analysis, frequency analysis and time frequency analysis.

The first method (TA) was based on a comparison of the computed statistical parameters of vibration in order to identify those parameters, which can endure the influence of flow fluctuation and can reveal valuable information corresponding to the impeller behaviour. Among the 8 statistical features that were investigated on this chapter, only a few parameters were capable to reveal less ambiguous patterns. Referring to figures 3.7 to 3.14, RMS, kurtosis, skewness and standard deviation showed a better performance than other features.

The second method (FA) studied on frequency components due to the condition of impeller and the fault severity. The location of the frequency peaks were utilized to identify between normal and faulty conditions. Signals are studied in low and high frequency ranges, respectively. The results (figures 3.18 and 3.19) proved that imbalance effects appear more in low frequency peaks, while the crack influence appear in higher frequency harmonics. Therefore, the amplitudes of the five dominant frequency components collected from the signals are used as conditional parameters to determine the health status of impellers (figure 3.20).

Finally WPT was applied in order to visualize system behaviour under time and frequency simultaneously. Vibration signals using db20 wavelet were decomposed up to 5 levels including 32 frequency bands with the length of 75Hz. Wavelet packet energy was used to evaluate the TFA method in this study (figure 3.28), which displayed that the WP energy has more potential to be used in condition classification compare to the other methods in this study.

4. Intelligent Diagnostics: Artificial Neural Networks (ANNs)

4.1. Introduction

This chapter presents fault detection methods. An artificial neural network is applied to the features, which are extracted from TA, FA and WPT techniques as described in previous chapter.

Feed forward neural network using backpropagation algorithm, is known as a well-known developed method in mapping the relationship between data sets. Hence, a three-layer feedforward ANN as proposed in chapter 1, is applied as an intelligent classification tool to identify and recognize the patterns between features and condition of system due to the data complexity. Also, ANN based condition estimation algorithm is elaborated, then it is verified with the extracted data from experimental system.

Four statistical parameters are selected as features in time domain signals, prominent frequency peaks in FA and finally energy of frequency subbands in WPT are chosen as significant data that characterise the corresponding system behaviour.

4.2. ANN Design and Performance

A three-layer feedforward ANN with an input layer, processing units (hidden layer) and an output layer is applied for the present study. A typical MLP network architecture is presented in chapter one, figure 1.7. Referring to equation 1.25, back-propagation in an ANN is considered as a simple method in mapping the non-linear relationship between inputs and the outputs of networks, and provides a supervised training for MLP networks. It applies a gradient descent technique on the error considered as function of the weights. Hence, there will be a gradient for weights to find the optimum value and minimize the error by moving the weight along the negative gradient of performance function. Back propagation algorithms comprise two steps, training and testing, respectively. Where, the network is to be trained by set of sample features, and tested in the second step using new data sets against the correct output to evaluate the accuracy of the network.

Therefore, in this chapter twelve measurements including 129600 sample points (data per each experiment) are collected from each condition under the fluctuating flow conditions. The required features are extracted from signals in three different domains, time, frequency and time-frequency domains, respectively.

The impeller feature set containing seven subsets of features represents impeller condition regarding to the 7 types of operating conditions (table 2.2). In addition, the data sets are divided into three independent subsets in order to be used for training, validating and testing the networks.

In order to train a MLP neural network, the first step is to define the number of inputs and outputs. Hence, three ANN structures are designed to study the performance of ANNs using features extracted from TDA, FA and TFA. Four features are selected from chapter 3 from the TA, representing impeller behaviour are RMS, kurtosis, skewness and standard deviation. Five frequency peaks corresponding to pump rotational speed (rpm) are selected from the FA representing as spectral features, and finally 32 features including frequency subband energy are selected from the TFA. Despite the fact that the input number varies in each domain, the number of outputs for the ANNs are the same based of the impeller condition. Therefore, seven outputs represent impeller condition (N, C1, C2, C3, U1, U2, and U3).

Furthermore, a binary format is used to define the defect types and severity levels in a 7 word binary format as shown in table 4.1. The output of the ANNs had to be one of the values as expressed in table below depending on the type of fault and severity level under consideration, hence, any other outcome not shown in the table are taken as an incorrect classification.

Table 4.1. Description of the ANN target output

Defect Description	Binary Code
Normal impeller	1000000
Crack level one (low)	0100000
Crack level two (medium)	0010000
Crack level three (high)	0001000
Unbalanced level one (low)	0000100
Unbalanced level two (medium)	0000010
Unbalanced level three (high)	0000001

The preliminary number of nodes in hidden layer can be estimated by equation 1.27 in section 1.3.5. Thereby, the hidden node number of the designed ANNs for TA feature sets (four features) must include 4 to 14 nodes, for FA features (5 features) the required hidden node number is 5 to 15, and for the features from WPT (32 features) the ANN must have 8 to 18 hidden nodes.

It is obvious that the node numbers and transfer function have a great impact on ANN performance. Non-linear and linear functions are suggested to be used in the hidden layer and the output layer respectively, however, there is no proof to identify the optimal number of nodes. Therefore, a set of training tests for different numbers of nodes in the specified range and three popular transfer functions such as, pure linear, hyperbolic tangent and logarithmic sigmoid functions, are carried out to evaluate the data in this study. Table 4.2 presents the ANN mean square error (MSE) based on WPT features. From the table it can be seen that logarithmic sigmoid function in hidden layer and linear function in output layer indicate the lowest MSE for the designed ANNs.

Table 4.2. Mean square error using different transfer function

Node number	Transfer function			
	(tansig,tansig)	(tansig,purelin)	(logsig,tansig)	(logsig,purelin)
4	0.01158	0.0886	0.1128	0.0861
6	0.0900	0.0765	0.1117	0.0628
8	0.0730	0.0847	0.1309	0.0624
10	0.0991	0.0430	0.109	0.0388
12	0.0686	0.1102	0.1581	0.0982
14	0.1425	0.1395	0.1608	0.0832
16	0.1182	0.0670	0.088	0.0311
18	0.0681	0.0985	0.0771	0.0315
Mean of RMS error	0.0969	0.0885	0.1185	0.0617

Also, a few more tests are performed to choose the most efficient number of nodes in hidden layer. Figure 4.1 and table 4.3 present the ANN performance in terms of prediction accuracy regarding the different node numbers. This process is being repeated 10 times for new testing data sets and the average of results are shown as below.

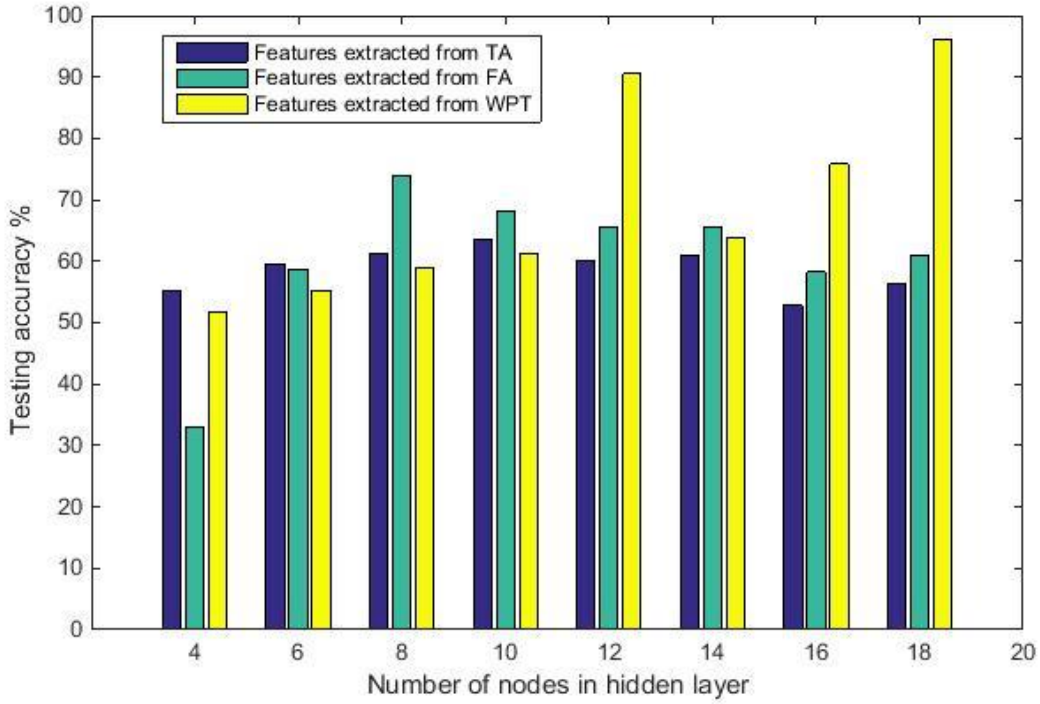

Figure 4.1. Performance comparison for different numbers of nodes in the hidden layer

Table 4.3. ANN accuracy with different numbers of nodes in the hidden layer

TA Features								
No. of nodes	4	6	8	10	12	14	16	18
Accuracy %	55.33	59.5	61.15	63.45	60.01	61.01	52.8	56.2
FA Features								
Accuracy %	33	58.64	73.84	68.22	65.45	65.56	58.25	60.9
WPT Features								
Accuracy %	51.74	55.29	59	61.30	90.51	63.82	75.81	96

The comparison results from table 4.3 suggest the efficient number of nodes in hidden layer to be selected as 10, 8 and 18 for features from signals in time, frequency and time-frequency domains respectively, which show the best estimations. Also, it can be seen that WPT features are more capable of training ANNs with higher performance accuracy, where, the testing accuracies of eight individual number of nodes vary from 51 to 96 %.

In addition, the average value of ANNs performance shows 12 % drop for frequency based features and 15 % drop of the network accuracy for features based on time signals.

Moreover, an investigation is provided to find the most effective learning algorithm that accelerates the learning process in neural networks. It is known as a difficult task which can be affected by various factors, such as complexity of networks, number of training sets and the target error or the required accuracy for outputs. The effectiveness of a learning algorithm is compared in terms of the time of training, optimum weights and the accuracy of network output. A comparison between three learning algorithm is provided using three different feature categories. Table 4.4 shows the averaged value of the network accuracy of new testing, the required time to train ANNs and the error of networks over 10 iteration with random initial weights. The learning algorithms in this comparison are Levenberg-Marquardt (LM), gradient descent and quasi Newton.

Table 4.4. Comparison of different learning algorithms on performance of ANNs

Learning algorithm	TA feature sets			FA feature sets			WPT feature sets		
	Time [s]	Accuracy %	Error	Time [s]	Accuracy %	Error	Time [s]	Accuracy%	Error
LM algorithm	7.64	91.02	0.0296	1	90.67	0.0306	2.51	95.32	0.0264
Gradient descent	1.7	61.39	0.0832	2.06	81.8	0.0578	1.58	92.97	0.0568
Quasi Newton	2.05	53.11	0.109	1.37	59.73	0.0802	74.54	93.35	0.0368

From the table above it can be seen that LM algorithm is the optimum algorithm for all three trained networks. LM algorithm results show lowest mean square error and highest output accuracy for new testing data sets.

Furthermore, there are some prominent facts that must be considered in an ANN design, such as data collection, data processing, normalization, network design, determination of the weights and bias values, network training and network validation. Two main issues are consider in validation process, first the required time to train a network and second is the network accuracy corresponding to the selected number of hidden layer nodes.

Hence, in order to verify the superiority of ANN based on WPT features, new data sets are provided to train, validate and test the ANNs. The backpropagation algorithm is implemented on data sets using LM algorithm as the base learning algorithm. Also the network performance and classification accuracy for each feature set from each methodology are examined.

Error plots and a confusion matrix that comprise convenient information, are used to evaluate the ANN performance. The following table 4.5 and figure 4.2 demonstrate the error plot and confusion matrix for each network. The maximum number of training epoch is set to 1000 for each training process. A sigmoid function is utilized as a nonlinear transfer function for hidden layer output and a linear function for the ANN output.

The error plot for each trained network shows how the network converged to the lowest output error over epochs of training. The training process stops at the point which is known as the best performance or the point before validation error starts to increase, which is an indication that the network starts overfitting the training data. In addition, confusion matrix tabulates the proportion of correct prediction for each seven possible classes (the impeller conditions) and shows the percentage of classes that are properly classified. It also shows the percentage of classes that are classified improperly. The correct classifications and the overall accuracy are shown in blue rectangles.

Figure 4.2. Training error curve of an ANN using TA features versus time

Table 4.5. Confusion matrix of an ANN trained using TA features

Output / Target	1	2	3	4	5	6	7	Accuracy
1	14.3 %	0	0.5 %	0	0	0.5 %	0	93.1 %
2	0	13.8 %	2.6 %	1.1 %	0	0.5 %	0	76.5 %
3	0	0	14.3%	1.1 %	0	0.5 %	0	87.5 %
4	0	0	0	10.6 %	0	0	0	100 %
5	0	0.5 %	0	1.6 %	14.3 %	0	0	87.1 %
6	0	0	0	0	0	12.7 %	0	100 %
7	0	0	0	0	0	0	14.3%	100 %
Accuracy	100 %	96.3 %	77.8 %	74.1 %	100	88.9 %	100 %	91 %

The first ANN is trained by applying statistical data derived from time domain signals. Figure 4.2 shows the error reduction over iteration of training. The mean square error at the lowest validation error is measured as 0.017 for the 26th iteration. The table 4.5 includes individual accuracy for each classes determined by the ANN, and also the percentage of correct and incorrect classifications are displayed. Nine misclassifications appeared in the table above and are individually presented in table 4.6.

Table 4.6. Incorrect classification of an ANN trained using TA feature sets

Correct class number	Misclassified class number		
1	3	7	
2	3	4	6
3	4	6	
5	2	4	

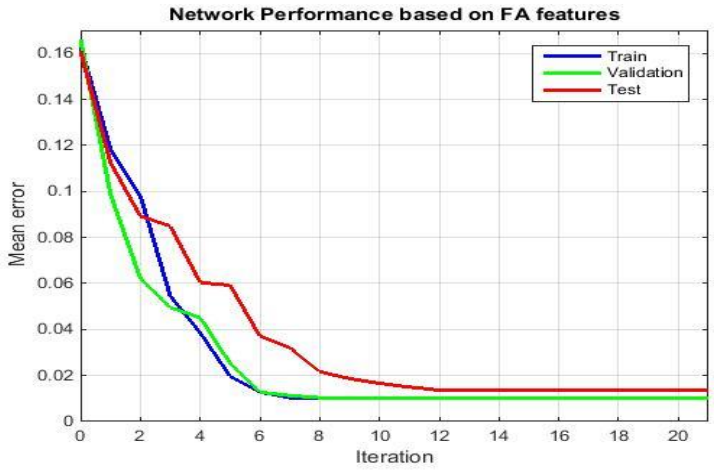

Figure 4.3. Training error curve of ANN using FA features versus time

Table 4.7. Confusion matrix of an ANN trained using FA features

Output / Target	1	2	3	4	5	6	7	Accuracy
1	14.3 %	0	0	0	0	0	0	100%
2	0	14.3%	0	0	2.4	0	0	85.7%
3	2.4%	0	9.5%	0	0	0	0	100%
4	0	0	0	14.3%	0	0	0	100%
5	0	0	4.8	0	11.9%	0	0	71.4%
6	0	0	0	0	0	14.3%	0	100%
7	0	0	0	0	0	0	14.3%	100%
Accuracy	100%	100%	66.7%	100%	83.3	100%	100%	92.9%

The second ANN is trained using features derived from signals in frequency domain. Five frequency peaks corresponding to rotational speed of the impeller and the vane passing frequency are selected and applied as input of the designed ANN. Figure 4.3 displays the lowest validation error in iteration range of 12 to 20 and the minimum value of 0.0165. Also table 4.7 shows 92.9% accuracy of the overall network performance. The misclassified classes are given as table 4.8.

Table 4.8. Incorrect classification of an ANN trained using FA feature sets

Correct class number	Misclassified class number
2	5
3	1
5	3

Figure 4.4 presents the behaviour of network error during training, validation and testing process. Thirty two energy values are extracted from different frequency bands after decomposition using wavelet analysis. Table 4.9 indicates an overall accuracy of 97.6% with only one misclassification, which class 7 (unbalanced impeller with severity of level 3) is being misclassified to class 2 (crack level 2).

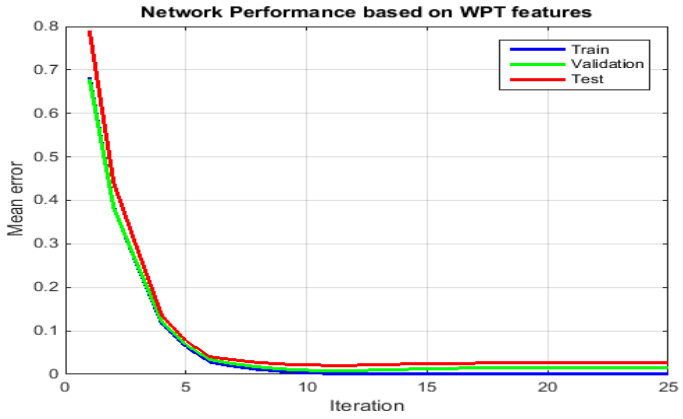

Figure 4.4. Training error curve of ANN using WPT features versus time

Table 4.9. Confusion matrix of an ANN trained using WPT features

Output / Target	1	2	3	4	5	6	7	Accuracy
1	14.3 %	0	0	0	0	0	0	100 %
2	0	11.9 %	0	0	0	0	0	100 %
3	0	0	14.3 %	0	0	0	0	100 %
4	0	0	0	14.3 %	0	0	0	100 %
5	0	0	0	0	14.3 %	0	0	100 %
6	0	0	0	0	0	14.3 %	0	100 %
7	0	2.4 %	0	0	0	0	14.3 %	85.7 %
Accuracy	100 %	83.3 %	100 %	100 %	100 %	100 %	100 %	97.6 %

By examining the results of above figures and tables, it can be stated that utilizing WPT feature sets to design and train artificial neural networks enhance the prediction accuracy of networks in compare to TA and FA feature sets. It also shows lower required time for training which is reasonable due to the lower iteration process of ANNs. In addition, the results denote a strong correlation between features due to rapid convergence of network while training progress.

4.3. Summary

In this chapter, some investigations were conducted in order to select the most accurate parameters and improve the performance of the designed ANNs. The most efficient transfer functions, learning algorithms and effective number of nodes in hidden layer were explored in these investigations; and the optimum number of nodes in the hidden layer corresponding to the network input features were determined. The performance of ANNs were found to be substantially better using logarithmic sigmoid function for hidden layer and linear function for output layer. In addition, the Levenberg-Marquardt was found to be the best algorithm for all three trained networks with rapid convergence, lowest mean square error and highest output accuracy.

Therefore, in order to investigate the effects of features on the ANNs performance, feature sets were taken out directly from experimental data from three types of signal analysis (time, frequency and time-frequency analysis). The extracted features were, namely statistical parameters, frequency peak ratios and subband energies. The results depict that ANNs are fairly reliable in impeller condition monitoring. The ANN performance improved considerably when WPT features are used (97.6%), whereas the ANN performance for the TA and FA based features achieved to 91% and 92.9% classification accuracy, respectively.

5. Conclusion

Maintaining equipment at the required condition and assuring reliable performance as well as improvement of safety are major concerns in asset integrity management field. Condition monitoring is a procedure that allows to identify signs of failures and perform efficient maintenance plans to eliminate the uncertainties in machine operation. In addition, vibration monitoring is known as an early detection tool in order to distinguish degradation from expected performance, which is superior to other CM techniques due to its high sensitivity and simplicity of implementation (P-F curve, chapter one). Vibration analysis provides substantial information regarding the operating condition of components and aid to remedy the problem. Therefore, it can be used to detect a wide range of fault conditions in rotating machinery such as imbalance, misalignment of internal shafts, looseness, cracked shaft, gear failures, rolling element bearing damages, motor faults and impeller issues.

The primary intention of the research reported on this dissertation was the investigation of the applicability of artificial neural network methodology on prognostics of mechanical defects and identification of fault categories of impeller in centrifugal pumps. The study focused on the contribution of feature extraction methods of vibration signals from pump impellers and the ANN performance of the extracted features. The second intention was to aid making maintenance decisions regarding the actual impeller condition. This leads to a transition from preventive maintenance to condition based maintenance, and also to improving the safety and reliability of pumping systems by reducing unexpected and catastrophic failures. Therefore, vibration analysis techniques are used as a principal tool to discriminate the impeller conditions under fluctuating flow conditions with the requirements of data collection, data processing, transformation and selection of essential features corresponding to the running condition.

This dissertation presents a study of current vibration analysis techniques to extract the required features, namely time, frequency and wavelet based features, respectively. Hence, a review was provided on the literature as below:

a) Vibration analysis aspects in condition monitoring of rotating machinery and the role of vibration analysis in fault diagnosis of pumping systems
b) Common potential failure modes of pumping systems and the related sources as well as the mechanisms involved in production of vibration

c) Common techniques in signal analysis such as time, frequency and time-frequency analysis with the particular attention being paid to non-stationary system conditions
d) Review of past research on the contribution of vibration based features and the intelligent interpretation, in order to study the vibration characteristics and define an efficient diagnostic feature regarding the impeller damage type
e) A detailed study on artificial neural networks and wavelet analysis methodology as well as common prominent parameters in each analysis method

Moreover, an experimental setup was developed to experimentally measure the impeller vibration. The experiment was performed using seven impeller conditions under fluctuating flow conditions which the pumping system was run for about 27 seconds over a range of varying flow rates (0 to 80 l/min). The variable flow rate caused different water impacts in the system and also simulated the cavitation phenomenon by reducing the water pressure at the pump inlet. In addition, cracks and imbalance were applied to the impellers including three level of severity as the artificial faults.

Subsequently, signal analysis techniques were applied on the measured vibration signals in order to identify the appropriate features corresponding to the conditions. The results from the time domain analysis denoted that only a few parameters follow a specific pattern. However, all the features did not necessarily expose individual and distinguishable information of the operating condition, some of the features gave ambiguous results due to the high interaction with the other features. Hence four parameters were selected from the graphical method that contained discernible information and represented the simulated conditions. These features were RMS, kurtosis, skewness and standard deviation.

Due to the fact that frequency spectra can render better visualization of the influence of damage and flow variation on the pump performance, the vibration signals were transformed to the frequency domain in the second step. The results stated that the imbalance defects excite the pump rotational frequency and its next four harmonics significantly. Conversely, crack effects appeared more on high order of harmonics of rotational speed frequency. Also, the results from flow fluctuation showed that the system was running under non-stationary conditions by changing the pump rotational frequency that made feature extraction in frequency domain difficult.

In the third step, wavelet analysis as a time-frequency decomposition method was applied in order to analyse the signals in both time and frequency domains. Since the WPT gives

high time and frequency resolutions for non-stationary signals, it was used in this study to decompose the signals up to level 5. Afterwards, each signal is divided into 32 frequency subbands covering 75 Hz of frequency length and the wavelet energy entropy of different frequency subbands were calculated to be used as the feature vector of each signal. The results therefore proved that the WPT method maps the pump vibration responses more accurately than other methods in diagnosis of impeller defects. It was also shown that the WPT reveals more detailed presentation of characteristic components such as the rotational speed frequency and the vane passing vibration.

Finally the efficiency of each method in feature extraction, which contains fundamental fault characteristic information, is evaluated. The collected data formed non-dimensional training data sets, were used to train the artificial neural networks (ANNs). The comparisons of different training algorithms, network hidden nodes and effectiveness of different transfer functions are also performed to select the most appropriate parameters. The results stated that the Levenberg-Marquardt algorithm with the aid of logarithmic sigmoid function in input hidden layer and pure linear function in output layer can provide more accurate predictions on impeller conditions. Moreover, a comparison of Daubechies wavelet in different ranges (2 to 35) was provided that the wavelet db20 was found to cover the frequency subbands more desirably due to less occurrence of frequency overlapping between different subbands.

Furthermore, a three layer feed forward ANN was trained off-line using Levenberg-Marquardt algorithm with logarithmic sigmoid and pure linear functions to validate the extracted features. Afterwards, the trained ANNs from each feature sets were applied to new experimental data to verify the feasibility of trained networks. The verifications showed that ANN prediction accuracy improved considerably using the energy based features of decomposed vibration signals. In addition, the comparison of the network accuracy based on WPT features with TA and FA based features pointed out lower mean square error, higher correlation between coefficients and faster training time for the ANNs based WPT features (WPT-ANNs). Thus it was concluded that the WPT-ANN models can save computational time and provide better diagnostic information, which can be effectively use for classification of impeller conditions under non-stationary conditions.

6. Future Work

Academic studies into how effective intelligent prognostic tools are at various levels of expertise, are in order. A great deal of work has been done on developing the technologies; however, more work needs to be done on how effective they really are.

The feature based ANN method developed and applied in this research. It has been shown the potential application of an ANN based wavelet analysis, and its superiority over current techniques for condition monitoring under non-stationary conditions.

However, this work has been concerned with off-line training networks and the presented methodology has been applied to the impeller fault diagnosis, which can be optimized as follow:

- More investigation of the other training algorithms to optimize the ANN performance, such as genetic algorithms and evolutionary algorithms.
- Applicability of feature selection techniques on reducing the redundancy of input features and chose the appropriate features and reducing the network computation time such as matching pursuit analysis and basis pursuit analysis.
- Comparison of WPT-ANN performance by other artificial intelligence methods for classification such as supervised machine learning method and unsupervised machine learning method.
- A deep exploration in other wavelet techniques and the relevant performance like short-time Fourier transform, Winger-Ville distribution and Hirbert-Huang transform.
- Performance on Daubechies wavelet on fault identification of other components and comparison with other wavelets, such as Meyer and Morlet wavelets.

Bibliography

Abdulkarem, W., Amuthakkannan, R. & Al-raheem, K.F., 2014. Centrifugal Pump Impeller Crack Detection using Vibration Analysis. In *2nd International Conference on Research in Science, Engineering and Technology*. pp. 206–211.

Ahonen, T., 2011. *Monitoring of Centrifugal Pump Operation by Frequency Converter*. Lappeenranta University of Technology.

Albraik, A., Althobiani, F. & Gu, F., 2012. Diagnosis of Centrifugal Pump Faults Using Vibration Methods. *Journal of Physics: Conference Series*, 364, p.012139.

Angelo, M., 1987. *Vibration Monitoring of Machines* No.1 ed., Bruel & Kjaer Technical Review.

Baydar, N. & Ball, A., 2001. A Comparative Study of Acoustic and Vibration Signals in Detection of Gear Failures using Wigner-Ville Distribution. *Mechanical Systems and Signal Processing*, 15(6), pp.1091–1107.

Berkouk, H. & Sadmi, T., 2014. Introduction to Wavelet Transform with Applications to DSP. In *Slideshare*. Available at: http://www.slideshare.net/hichamberkouk/introduction-to-wavelet-transform-with-applications-to-dsp?qid=7bafcfde-ce28-4b3e-8c22-8eee49488c8b&v=default&b=&from_search=2.

Birajdar, R., Patil, R. & Khanzode, K., 2009. Vibration and Noise In Centrifugal Pump Sources And Diagnosis Methods. In *3rd International Conference on Integrity, Reliability and Failure*. pp. 20–24.

Bray, D.E. & Stanley, R.K., 1997. *Non-Destructive Evaluation a Tool in Design, Manufacturing and Services* Revised. N. Stanton & A. Demby, eds., Boca Raton.

Brownlee, J., 2013. A Tour of Machine Learning Algorithms. Available at: http://machinelearningmastery.com/a-tour-of-machine-learning-algorithms/ [Accessed July 10, 2015].

Chebil, J., Noel, G. & Mesbah, M., 2009. Wavelet Decomposition for the Detection and Diagnosis of Faults in Rolling Element Bearings. *Journal of Mechanical and Industrial Engineering*, 3(4), pp.260–267.

Chen, H.X.A., Chua, P.S.K. & Lim, G.H., 2008. Fault Degradation Assessment of Water Hydraulic Motor by Impulse Vibration Signal with Wavelet Packet Analysis and Kolmogorov Smirnov Test. *Mechanical Systems and Signal Processing 22*, 22, pp.1670–1684.

Connection Technology Center Inc, 2012. Beginning Vibration Analysis. *CTC University*. Available at: https://www.ctconline.com/__ctc_university.aspx.

Davies, D., 2015. RMS from Time History and FFT Spectrum. Available at: http://blog.prosig.com/2015/01/06/rms-from-time-history-and-fft-spectrum/ [Accessed July 7, 2015].

Deepak Prabhakar, P. & Jagathy Raj, V.P., 2014. CBM , TPM , RCM and A-RCM - A Qualitative

Comparison of Maintenance Management Strategies. *International Journal of Management & Business Studies*, 4(3), pp.49–56.

Domingos, P., 2012. A Few Useful Things to Kow about Machine Learning. *Communications of the ACM*, 55(10), p.78.

El-Thalji, I. & Jantunen, E., 2015. A Summary of Fault Modelling and Predictive Health Monitoring of Rolling Element Bearings. *Mechanical Systems and Signal Processing*, 60-61, pp.252–272.

Gao, R.X. & Yan, R., 2011. *Wavelets*, Boston, MA: Springer US. Available at: http://link.springer.com/10.1007/978-1-4419-1545-0.

Gill, T., Wahlin, B. & Replogle, J., 2011. Venturi Meters Constructed with Pipe Fittings : An Under-Appreciated Option for Measuring Agricultural Water. In *Emerging Challenges and Opportunities for Irrigation Managers Albuquerque, New Mexico*.

Girdhar, P., 2004. *Practical Machinery Vibration Analysis and Predictive Maintenance* C. Scheffer & P. Girdhar, eds., Elsevier.

Graney, B.P. & Group, M., 2011. Pump Vibration Analysis. *Pumps and Systems*, 4. Available at: http://www.pumpsandsystems.com/topics/instrumentationcontrols/pump-vibration-analysis [Accessed June 30, 2015].

H.Tackett, H., Cripe, J.A. & Dyson, G., 2008. Positive Displacement Reciprocating Pump Fundamentals, Powe and Direct Acting Types. *Proceeding of the twenty fourth international pump users symposium*, pp.45–58. Available at: http://turbolab.tamu.edu/proc/pumpproc/P24/.

Heyns, P.S., 2008. *Mechanical Vibration measurement and analysis*, University of Pretoria.

Heyns, P.S., 2007. Tool condition monitoring using vibration measurements - a review. *WCEAM-CM2007, the Second World Congress on Engineering Asset Management and Fourth International Conference on Condition Monitoring, Harrogate*, 49(8), pp.447–450.

Jantunen, E., 2002. A summary of methods applied to tool condition monitoring in drilling. *International Journal of Machine Tools and Manufacture*, 42(9), pp.997–1010.

Jardine, A.K.S., Lin, D. & Banjevic, D., 2005. A review on machinery diagnostics and prognostics implementing condition-based maintenance. *Mechanical Systems and Signal Processing*, 20(7), pp.1483–1510.

John, A. & Putman, M.A., 2007. *Signal Processing Techniques*, Available at: https://www.eeginfo.com/research/researchpapers/Signal_Processing.pdf.

Kankar, P.K., Sharma, S.C. & Harsha, S.P., 2011. Fault Diagnosis of Ball Bearings using Continuous Wavelet Transform. *Applied Soft Computing Journal*, 11(2), pp.2300–2312.

Karlik, B. & Olgac, A., 2010. Performance Analysis of Various Activation Functions in Generalized MLP Architectures of Neural Networks. *International Journal of Artificial Intelligence and Expert Systems (IJAE)*, (1), pp.111–122.

Klapetek, P., Necas, D. & Anderson, C., 2015. Gwyddion User Guide, Chapter 4. Data Processing and Analysis, Wavelet Transform. Available at: http://gwyddion.net/documentation/user-guide-en/ [Accessed July 10, 2015].

Lauro, C.H. et al., 2014. Monitoring and Processing Signal Applied in Machining Processes: A review. *Measurement*, 58, pp.73–86.

Lee, D.T.L. & Yamamoto, A., 1994. Wavelet Analysis : Theory and Applications. *Hewlett - packard journal*, (December), pp.44–52.

Liao, W., Gao, S. & Liu, Y., 2009. Fault Diagnosis of Engine Based on Wavelet Packet and RBF Neural Network. *2009 Second International Conference on Intelligent Computation Technology and Automation*, pp.521–524.

Liu, L. & Ganeriwala, S., 2012. Diagnosing Tiny Bubbles. Available at: http://reliabilityweb.com/articles/entry/diagnosing_tiny_bubbles [Accessed September 10, 2015].

Lorenzo, F. De & Calabro, M., 2007. Kurtosis : A Statistical Approach to Identify Defect in Roller Bearings. *2nd International Conference on Marine Research and Transportation*, 3, pp.17–24.

Loughlin, P., Cakrak, F. & Cohen, L., 2000. Conditional Moments Analysis of Transients With Application To Helicopter Fault Data. *Mechanical Systems and Signal Processing*, 14(4), pp.511–522.

M J . Neale & Woodley, B.J., 1978. Condition Monitoring Methods and Economics handbook. In *Bruel & Kjaer*. Denmark.

Maind, S.B. & Wankar, P., 2014. Research Paper on Basic of Artificial Neural Network. *International Journal on Recent and Innovation Trends in Computing and Communication*, 2(1), pp.96–100.

Mesbah, M., Boashash, B. & Mathew, J., 2003. Time Frequency Based Machine Condition Monitoring and Fault Diagnosis. In B. Boashash, ed. *Time Frequency Signal Analysis and Processing: A Comprehensive Reference*. Elsevier Ltd, pp. 671–682.

Moubray, J., 1992. *Reliability-centred maintenance* 2nd ed., New York, N.Y. : Industrial Press, c1992.

Nandi, A.K., Liu, C. & Wong, M.L.D., 2013. Intelligent Vibration Signal Processing for Condition Monitoring. In *Proceedings of the International Conference Surveillance 7*. Chartres, France, pp. 1–15.

Patel, J., Patel, V. & Patel, A., 2013. Fault Diagnostics of Rolling Bearing based on Improve Time and Frequency Domain Features using Artificial Neural Networks. *International Journal for Scientific Research & Development*|, 1(4), pp.781–788.

Pentax Co., 2013. Product catalogue. Available at: http://www.pentax-pumps.it.

Phinyomark, A., Limsakul, C. & Phukpattaranont, P., 2009. Evaluation of mother wavelets based on robust EMG feature extraction using wavelet packet transform. In *13th Anual symposium*

on computational science and engineering. Kasetsart University, pp. 333 – 339.

Qu, J., Zhang, Z. & Gong, T., 2016. A Novel Intelligent Method for Mechanical Fault Diagnosis based on Dual-Tree Complex Wavelet Packet Transform and Multiple Classifier Fusion. *Neurocomputing*, 171, pp.837–853. Available at: http://linkinghub.elsevier.com/retrieve/pii/S0925231215009960.

Randall, R.B., 1974. Vibration signature analysis - techniques and instrument systems. In *Noise, Shock and Vibration Conference*. Melbourne, pp. 1 – 6.

S.DEORE, K. & A. KHANDEKAR, M., 2014. Bearing Fault Detection in Induction Motor Using Time Domain Analysis. *International Journal of Advanced Research in Electrical, Electronics and Instrumentation Engineering*, 3(7), pp.10702–10707.

Sakthivel, N.R., Sugumaran, V. & Babudevasenapati, S., 2010. Vibration based fault diagnosis of monoblock centrifugal pump using decision tree. *Expert Systems With Applications*, 37(6), pp.4040–4049.

Samanta, B., 2004. Gear fault detection using artificial neural networks and support vector machines with genetic algorithms. *Mechanical Systems and Signal Processing*, 18(3), pp.625–644.

SGS, C., 2015. Asset management policies. Available at: www.sgs.com/aim [Accessed May 1, 2015].

Shreve, D.H., 1995. Signal Processing for Effective Vibration Analysis. *IRD Mechanalysis Inc, Columbus*. Available at: http://www.irdbalancing.com/.

Sifuzzaman, M., Islam, M.R. & Ali, M.Z., 2009. Application of Wavelet Transform and its Advantages Compared to Fourier Transform. *Journal of Physical Sciences*, 13, pp.121–134.

Taneja, S., 2013. Effect of Unbalance on Performance of Centrifugal Pump. *International Journal of Scientific & Technology Research*, 2(8), pp.56 – 60.

Toth, L., 2013. On Finding Better Wavelet Basis for Bearing Fault Detection. *Acta Polytechnica Hungarica*, 10(3), pp.17–35.

Unal, M., Onat, M. & Demetgul, M., 2014. Fault Diagnosis of Rolling Bearings using a Genetic Algorithm Optimized Neural Network. *Measurement*, 58, pp.187–196.

Wang, Y. et al., 2015. Detection of Weak Transient Signals based on Wavelet Packet Transform and Manifold Learning for Rolling Element Bearing Fault Diagnosis. *Mechanical Systems and Signal Processing*, 54-55, pp.259–276.

White, F.M., 2011. *Fluid mechanics* 7th ed., New York: McGraw Hill.

Xing, Y.F. et al., 2015. Sound Quality Recognition using Optimal Wavelet-Packet Transform and Artificial Neural Network Methods. *Mechanical Systems and Signal Processing*, pp.1–18.

Yang, H., Mathew, J. & Ma, L., 2003. Vibration Feature Extraction Techniques for Fault Diagnosis of Rotating Machinery: A Literature Survey. In *Asia- Pacific Vibration Conference, 12-14 November, Gold Coast, Australia*. pp. 12–14.

Zhang, M., Li, K. & Hu, Y., 2010. Classification of Power Quality Disturbances Using Wavelet Packet Energy Entropy and LS-SVM. *Energy and Power Engineering*, 2, pp.154–160.

Zhao, X.M. et al., 2010. Vibration-based fault diagnosis of slurry pump impellers using neighbourhood rough set models. *Proceedings of the Institution of Mechanical Engineers, Part C: Journal of Mechanical Engineering Science*, 224(4), pp.995–1006. Available at: http://pic.sagepub.com/lookup/doi/10.1243/09544062JMES1777.

Zouari, R. & Menad, S.S., 2004. Fault Detection System for Centrifugal Pumps using Neural Networks and Neuro-Fuzzy Technique. In *Surveillance 5 Cetim Senlis 11–13 October 2004*.

Appendix A: Solidworks Drawing of Venturi Meter